# Multiplexing of Extrinsic Fabry-Perot Optical Fiber Sensors for Strain Measurements

By

David Geib

Thesis submitted to the faculty of the

Virginia Polytechnic Institute and State University

In partial fulfillment of the requirements for the degree of

Master of Science

In

Electrical Engineering

Dr. Anbo Wang, Chair

Dr. A. Safaai-Jazi

Dr. M.P. Singh

August 4th, 2003

Blacksburg, Virginia

Keywords: Multiplexing, Fabry-Perot, Fiber Optic Sensors, Strain, Whitelight, Fourier Analysis, Crosstalk

# Multiplexing of Extrinsic Fabry-Perot Optical Fiber Sensors for Strain Measurements

By

David Geib

## (Abstract)

Elevators are a necessary component of the modern urban and suburban life. The guide rails the car and counterweight move on are the most sensitive parts when it comes to de-habilitating damage that can be caused by an earthquake. Conventional sensors are becoming obsolete in sensing for today's multistory buildings because they don't monitor the structural health of the guide rails. This sensing task falls into the fiber sensing niche market because of a fiber sensor's ability to be multiplexed. Previous work by Taplin and Jackson showed demodulation of the interference spectrum of two Fabry-Perot cavities using Fourier analysis. The goal of this thesis research is to use Fourier analysis to demodulate the spectrum of multiplexed extrinsic Fabry-Perot fiber interferometers for strain measurements. Comparisons of fiber, foil, and theoretical strains are made. Also, experiments showing the system's air-gap stability and crosstalk are provided.

# Acknowledgements

First I would like to thank Virginia Tech for giving me the opportunity to study here. I am very proud to a part of the graduate school and hope my contributions help enhance the reputation of this great institution. I would also like to thank he ECE department for accepting me to be a GTA. Not only did it help me with my public speaking, but it also led me to meeting my advisor Dr. Anbo Wang.

Most importantly I would like to thank Dr. Wang for accepting me as one of his graduate research assistants. I consider myself very lucky and privileged to work in the Center for Photonics Technology. The other members on my committee also deserve recognition, thank you Dr. M.P. Singh for choosing CPT to undertake the sensing part of your experiment, and thank you to Dr. Safaai-Jazi for your support and guidance.

Personally I would like to thank my family. Their support was crucial throughout my entire education. I would also like to thank my friends for all there help in and outside lab. Special thanks to Yizheng for coating the fibers for me, and to Ming Han and Dae Woong Kim for all their help. Finally I want to thank my girlfriend April for being very patient through my time here and also for all her support and motivational talks.

# Table of Contents

# List of Figures

# List of Tables

# Chapter 1: Introduction

Elevators are an important part of modern day life, whether they are used for transporting people or tangibles. In hospitals elevators are crucial in the fight to preserve life. Some of these elevators are located near seismic hotspots, and can be easily damaged rendering them useless during their greatest need. Therefore a device is needed that can ascertain the safety and integrity of the elevator structure after a seismic event.

The elevator structure is basically composed of a car and a counterweight that are connected with cables through a pulley on the roof. The counterweight is used to balance the car and up to fifty percent of the rated load of the car. Both the car and counterweight travel on two vertical guide rails via three rubber tires. These rails and roller guides have shown to be the most vulnerable during earthquakes, especially for the heavier counterweight[1].

Current seismic sensors consist of one seismic switch per building and one or more displacement switches on the counterweight. The seismic switch is an accelerometer with a threshold of 0.15 times the force of gravity, and is intended to give warning of an earthquake[2]. The displacement switch is set up so if the counterweight moves off the guide rails, it will detect it and make the car go to the nearest floor slowly. The counterweight displacement switch is shown in Figure 1.1[1]. These sensors are becoming obsolete, due to the size of buildings. A small oscillation on the ground can cause very large oscillations at the roof and damage essential components without the sensor being activated. Also during an earthquake there is a possibility that the guide rails could be damaged without it being known exactly where.
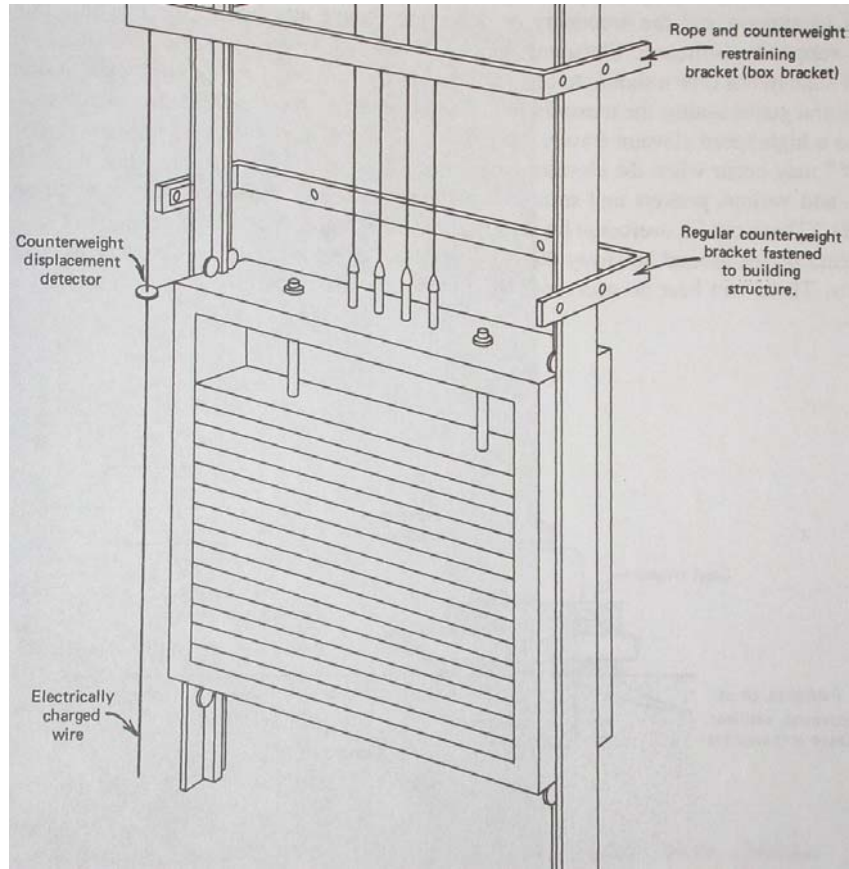
Figure 1.1 – Counterweight With Displacement Ring Sensor[1]

Fiber optic sensors are now becoming a more viable option because of their many advantages to conventional electric sensors in certain situations. The multiplexing ability of fiber sensors makes them a prime candidate for a sensing system in a multistory elevator shaft. This research is intended to study the possibility of multiplexing fiber optic Fabry-Perot Interferometers using Fourier analysis for demodulation.

## 1.1 Strain and Gauge Length

When a force is applied to a material, it undergoes a change in its physical shape or strain. Strain, $\varepsilon$, is mathematically defined as a ratio of the change in length $\Delta L$ over the total length L,

$$\varepsilon = \frac{\Delta L}{L} \qquad (1.1)$$

Measurement of strain can be done in a variety of ways. A common way is by bonding a sensor on the material so the same ratio of strain is transferred to the sensor. Both electrical and fiber optic sensors work in this fashion.

## 1.2 Cantilever Beam Strain Analysis

Although there are several methods to create strain on a test piece, a cantilever beam setup was chosen to better represent the elevator beam that will be tested later. Figure 1.2 shows a cantilever beam setup with some labeled parameters for Equation 1.2.
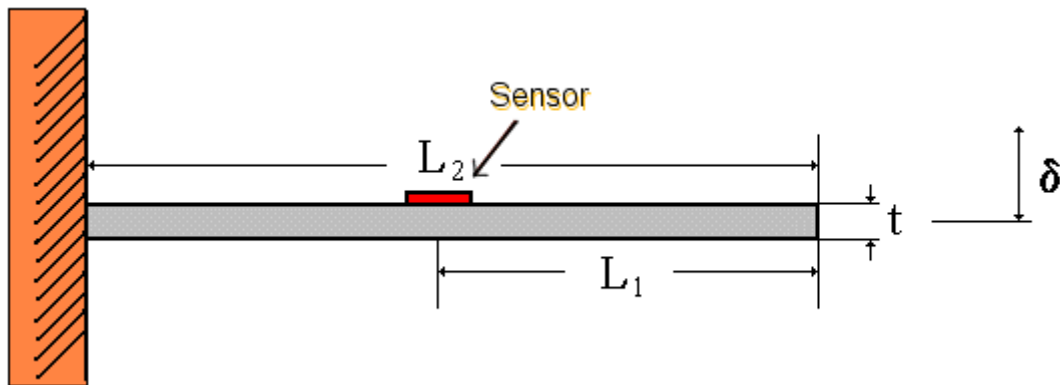


Figure 1.2 – Cantilever Beam Diagram.

The strain can be found at any point on the beam from the equation,

$$\varepsilon = \frac{3L_1 t}{2L_2^3}\delta \qquad (1.2)$$

where $L_1$ is the length from the deflected end of the beam to the sensor, t is the thickness, $\delta$ is the beam tip deflection, and $L_2$ is the length of the beam[3].

## 1.3 Foil Strain Gauges

There are a few ways to measure strain electronically, one is by taking advantage of the effects strain has on the resistance of a wire. A wire strain gauge is a length of wire wrapped back and forth between two pieces of polymer. The wire is wrapped in such a way as to have as much of the wire parallel with the force creating the strain. This

wrapping technique amplifies the effects the strain has on the wire's resistance. A foil strain gauge is just like the wire strain gauge except the wire is now a printed circuit that is etched out of foil. Figure 1.3 is a picture of a foil strain gauge[4].
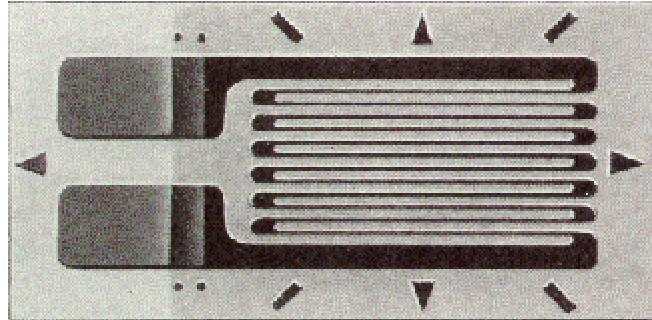


Figure 1.3 – Foil Strain Gauge[4]

## 1.3.1  Resistive Theory

Both the wire and foil strain gauges work on the changes of resistance of the wire it is made from. The resistance of a material is inversely proportional and highly sensitive to its cross sectional area and is given as,

$$R = \rho \frac{L}{A} \tag{1.3}$$

where R is the resistance, $\rho$ is the resistivity of the material, L is the length of wire, and A is the cross sectional area. As the strain gauge is stretched or compressed, the wire's volume stays nearly constant and therefore the cross sectional area changes. When the area changes the resistance will change, increasing as the area decreases, and decreasing as the area increases. A secondary effect in ordinary conductors resulting from the strain is the change in the resistivity of a material. However the change is negligible, and can be ignored in most metal conductors[5].

The relationship between the resistance and strain is the sensitivity factor or K, and is given by the equation,

$$K = \frac{\Delta R / R}{\Delta L / L} = \frac{\Delta R / R}{\varepsilon} \tag{1.4}$$

4

where R is the resistance, L is the length, and ΔL/L is the strain.  Typical values range from 2 to 2.2 and depend on the material used for the wires[5].  For the foil strain gauges used in this experiment the manufacturer gives the K factor as 2.105.

## 1.3.2  Wheatstone Bridge

From equation 1.4 and a given K value, it is clear that all one needs is a way to monitor the resistance of the gauge to calculate the strain.  This is where a Wheatstone Bridge comes into play.  In 1843 Charles Wheatstone invented a circuit that could be used to find unknown resistances of a load[6].  A diagram of a quarter Wheatstone bridge is shown in Figure 1.4.  It is known as a quarter Wheatstone bridge because only one the four resistors is a strain gauge.



Figure 1.4 – Wheatstone Bridge Diagram[5].

When resistors $R_1$, $R_2$, $R_3$, and the foil gauge are equal in resistance the potential across points B and D of the circuit will be zero volts.  However when there is a change in the resistance of the foil gauge, there will be a potential difference across points B and D[5]. The strain equation for a quarter Wheatstone bridge is,
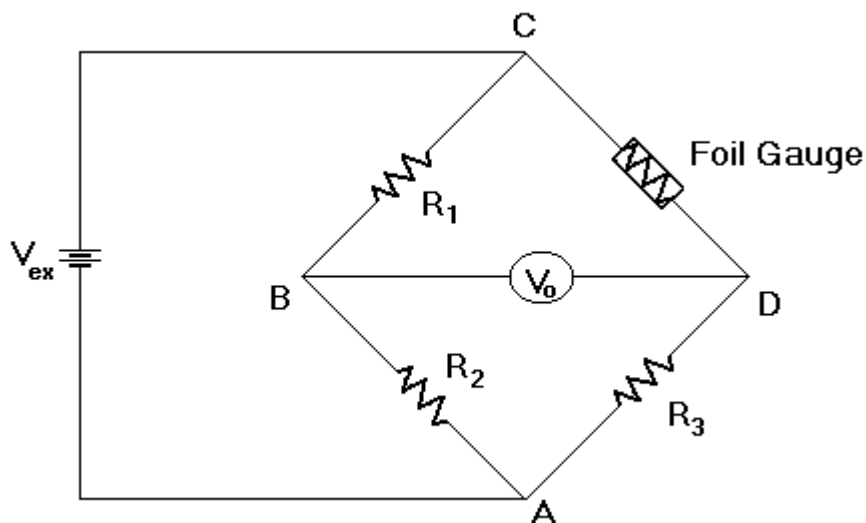
$$\varepsilon = \frac{4V_0}{V_{ex}KG} \tag{1.5}$$

where K is the sensitivity factor, $V_{ex}$ is the input or excitation voltage, $V_o$ is the output voltage from the Wheatstone bridge, and G is the gain. The Wheatstone bridge can also be setup in a half bridge configuration for temperature compensation. In a half bridge, resistor $R_3$ is replaced by a foil strain gauge that is isolated from strain, but still affected by temperature effects. However, in a laboratory environment the temperature effects are negligible and therefore use of a quarter bridge is acceptable.

### 1.3.3  Advantages and Disadvantages of Foil Strain Gauges

An advantage of the foil strain gauge is that it is mass-produced making it cheap, reliable, and relatively small. Also, the workings of the foil strain gauge are simple yet accurate. The resolution of a foil strain gauge is 0.1 μstrain with a maximum strain of 200,000 μstrain[4]. The inherent temperature compensation of the Wheatstone bridge adds to the advantages of the foil strain gauge system. The foil strain gauge also has very little transverse sensitivity compared to wire strain gauges, because the large amounts of area at the turns on the foil gauge prevent perpendicular strains from affecting the performance[5].

A disadvantage of foil strain gauges is their inability to be multiplexed. Each sensor is attached to its own conditioning equipment and in order to get data from multiple spots, a dedicated system is needed for each one. Also, because the strain gauges are electrical they are susceptible to electromagnetic interference.

Mounting the sensors is also a problem. The test piece must be sanded and washed with great attention to detail as no to contaminate the epoxy. For accurate measurements the gauge must be fixed to the test piece very securely and as close as possible, which means using a clamp to get a very thin and uniform amount of epoxy. Finally the lead wires must be soldered in place, cleaned of excess flux, and a protective coating applied. With some practice these tasks can be mastered for a simple laboratory test piece, however if

the test piece is not readily accessible or removable some of the tasks can be nearly impossible.

The epoxy itself can also be a problem because of curing temperatures and times. Also the epoxy is not a perfectly elastic material. The sensors can undergo creep, which is a gradual lowering of the strain that acts on the gauge. Creep can occur due to a bad bond, or from steady or highly repetitive strain. Higher operating temperatures can also weaken the epoxy and cause creep if special high temperature epoxy is not used[7].

For highly precise measurements hysteresis is another disadvantage of foil strain gauges. Hysteresis is when a high amount of strain is applied and then released from the strain gauge. The gauge will seem deformed and will have a higher resistance value at zero strain than initially. A similar effect will happen in the opposite direction and setting up a hysteresis loop. The loop can be narrowed to negligible values by repeatedly stressing the gauge in opposite directions. However, A typical value of error is 0.1 percent and usually can be ignored for measurements less than 1500 microstrain[5]. A plot of a histerisis loop is shown in Figure 1.5.
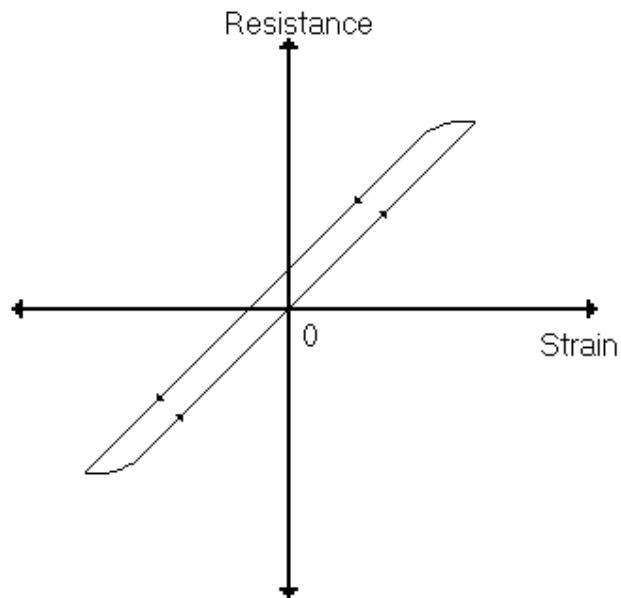


Figure 1.5 – Hysterisis Loop

# Chapter 2: Fiber Sensors

## 2.1 Fiber Sensors

Recent advances in fiber optic technology have revolutionized the telecommunications industry. The potential to carry gigabits of information at the speed of light sparked an explosion in research of optical fibers. The race for a loss-less fiber began. Progress came so fast that fiber optic technology was in its fifth generation in only 25 years[8]. Soon it was discovered that, with material loss almost disappearing, and the sensitivity for detection of the losses increasing, one could sense changes in phase, intensity, and wavelength from outside perturbations on the fiber itself. Hence fiber optic sensing was born.

## 2.2 Benefits of Fiber Sensing

Fiber sensors posses many advantages over conventional electronic sensors, the first being their sensitivity. A fiber optic interferometer has a resolution that is 4 orders of magnitude better than a conventional displacement sensor[9]. Most of the advantages for fiber sensors lye in the area where conventional sensors cannot go. Not only are fiber sensors smaller, but also they are more resistant to harsh environments. They are non-electrical and therefore are not subject to electromagnetic interference. A glass composition keeps fiber sensors immune to most corrosive and high temperature environments. The low loss property of the glass permits remote sensing from a great distance. Finally, fiber optic sensors are very versatile to what they can collect data for, and are only limited by an engineers creativity to convert what they want to sense into one of the many ways a fiber sensor can.

## 2.3 Choosing A Fiber Sensor

There are many different types of sensors that can produce data for strain, temperature, electric and magnetic fields, and most other physical properties. However, each sensor also has properties that make them more suited for certain types of measurements. The following paragraphs will explain a variety of sensors and how they work, and finally which sensor was chosen for this experiment.

## 2.3.1 Intrinsic and Extrinsic Sensors

Most sensors can be classified into two categories, intrinsic and extrinsic. The intrinsic sensor uses the entire fiber or a section of the fiber as the sensing device. Perturbations act on the fiber and the fiber in turn changes some characteristic of the light being guided in it. The light never leaves the fiber, which makes these sensors good for dirty environments. The intrinsic sensor can also be used for distributed sensing, such as in smart structures. The extrinsic fiber sensor has a separate device to alter the light. The fiber just acts as a means of getting the light to the sensing location. This style offers many ways to achieve the sensing desired, because one can add things that may be more sensitive than the fiber alone[10].

## 2.3.2 Intensity Based Sensors

Another way to categorize fiber optic sensors is how they achieve their sensing. The first and most basic is the intensity-based sensor, which relies on the signal undergoing some loss. A simple sensor can be made by having an apparatus to convert what is being measured into a force that bends the fiber and causes attenuation of the signal. Other ways to attenuate the signal is through absorption or scattering off a target. The intensity-based sensor requires more light and therefore usually uses multimode large core fibers[9].

### 2.3.3 Wavelength Modulated Sensors

The next category is wavelength-modulated sensors. These sensors use changes in the wavelength of light to do their sensing. Examples of wavelength-modulated sensors are fluorescence sensors, phosphorescence sensors, and the most popular, the Bragg grating sensor.

In the fluorescence and phosphorescence sensors the source light is absorbed by some material and then emitted at a different wavelength. The difference between fluorescence and phosphorescence is the length of time after excitation the emitted light can be detected[11]. These emissions can be temperature or radiation sensitive, and hence can act as a sensor[9].

The Bragg grating sensor uses a periodic refractive index change in the core to filter a resonant wave out of the source spectrum. The grating is usually written on a fiber using an ultraviolet laser. The ultraviolet light reacts with the Germanium doped core and causes the refractive index to increase. The resonant wavelength condition is given as

$$\lambda_r = 2n\Lambda \qquad (2.1)$$

where $\lambda_r$ is the resonant wavelength, n the refractive index of the fiber core, and $\Lambda$ is the length of one period of the grating. Only the light that meets this resonant condition will be reflected back to the source. Bragg gratings are extremely sensitive to mechanical strain[12]. Changes of a few nanometers can be easily detected due to the fact that the wavelength of light is on the same order. However, Bragg gratings are also very sensitive to thermal expansion induced strains. A temperature change of one degree Celsius results in a 0.01 nm shift of the resonant peak. Also, crosstalk can be a problem when a large amount of sensors are multiplexed. As the reflectivity of the Bragg grating increases multiple reflections can slow transmission and interfere with time dependent

systems.  Shadowing is another variation of crosstalk and is the result of the signal passing through the first few gratings twice[9].

## 2.3.4 Phase Modulated Sensors

The final category is phase-modulated or interferometric sensors.  There are three types of interferometer that can be used for displacement measurement, the Mach-Zender, the Michelson, and the Fabry-Perot.  The principle of an interferometer is the light is split into two beams, one beam is exposed to the sensing environment and undergoes a phase shift and the other is isolated from the sensing environment and is used for comparison. When the beams are recombined they interfere with each other. The Mach-Zender and Michelson interferometers are shown in Figures 2.1 and 2.2 respectively.  The major difference between the two is that the light passes through the sensing region twice in the Michelson interferometer and therefore it is more sensitive[9].  Although both interferometers are excellent at displacement measurements, their use of separate reference fibers makes them less attractive for multiplexing.
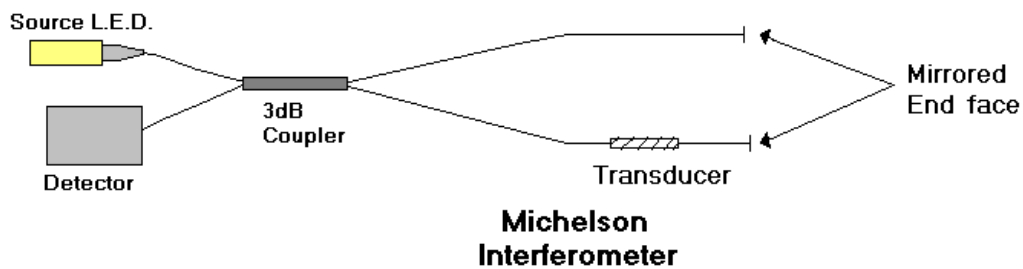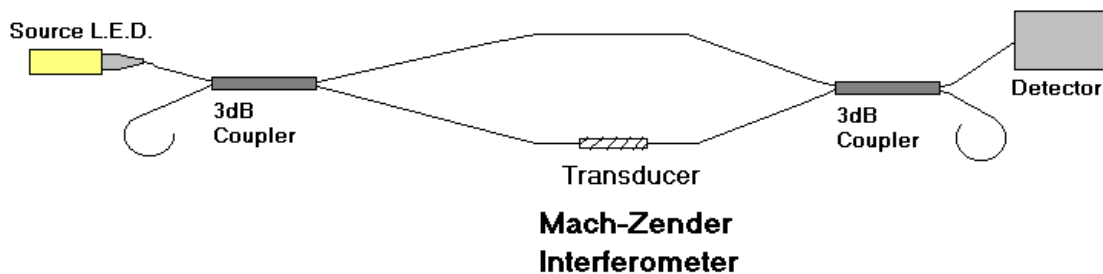
Figure 2.1 – Michelson Interferometer Diagram[9]

Figure 2.2 – Mach-Zender Interferometer Diagram[9]

This leaves our last sensor, the Fabry-Perot Interferometer, as our final choice for the strain sensor.

## 2.4 Fabry-Perot Sensors

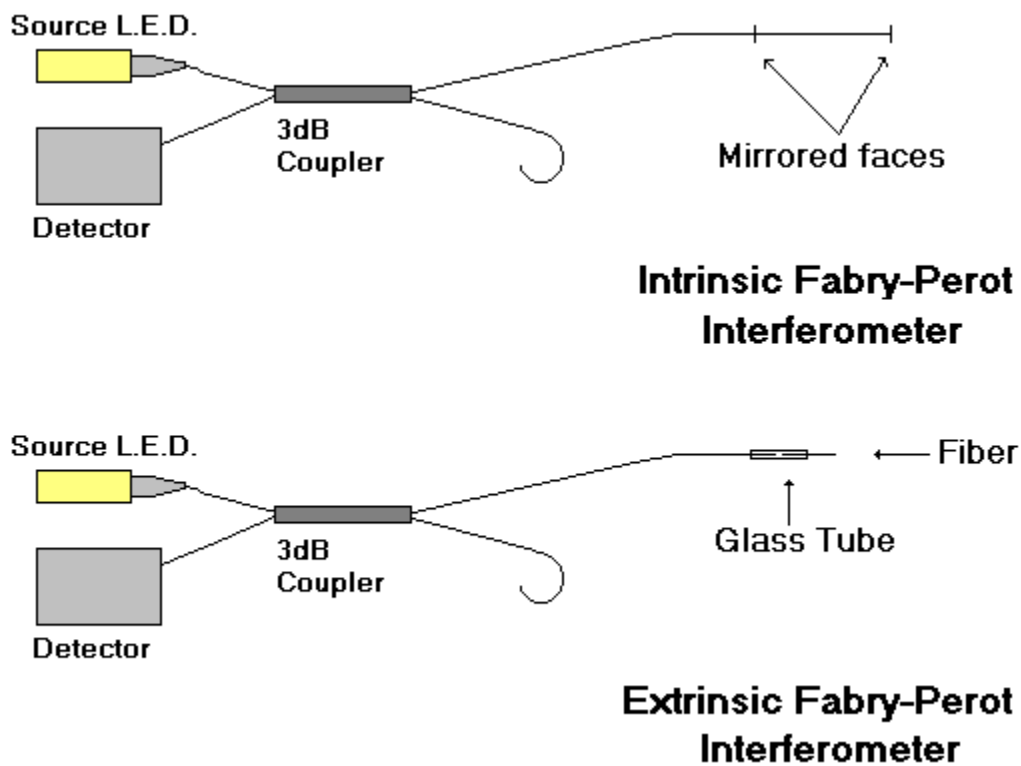The Fabry-Perot sensor can be either intrinsic or extrinsic as shown in Figure 2.3.



Figure 2.3 Diagram of Intrinsic F-P Sensor (top) and Extrinsic F-P Sensor (Bottom)[9].

For this experiment the extrinsic Fabry-Perot interferometer (EFPI) was used. Composed of a glass capillary tube and a piece of fiber the EFPI is small and easily constructed. As shown in Figure 2.4, the EFPI achieves two-beam interference with only one fiber.
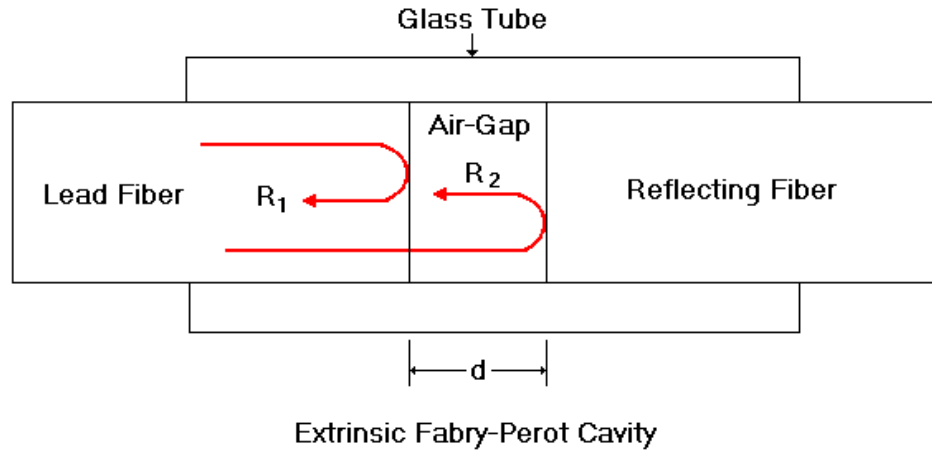
Figure 2.4 – Close Up of Fabry-Perot Sensor.

Light from a broadband source reaches the sensor and undergoes a partial reflection of approximately four percent off the lead fiber end face. The rest of the light is transmitted into the air-gap. The light then reflects off the reflecting fiber face and travels back through the air-gap and re-enters the lead fiber. The second reflection travels an extra distance of twice the air-gap length and hence has a phase shift. Since the light is composed of many wavelengths, and the air-gap is large compared to them, there will be more than one wavelength that undergoes interference. Thus, the return spectrum will have an interference pattern where some wavelengths interfere constructively and some de-constructively. Another advantage from the air-gap being large compared to the wavelength is that very small changes in the air-gap can be detected, and air-gaps that differ by at least 0.1 nm in length will have a different interference spectrum. Figure 2.5 shows an example spectrum[13].
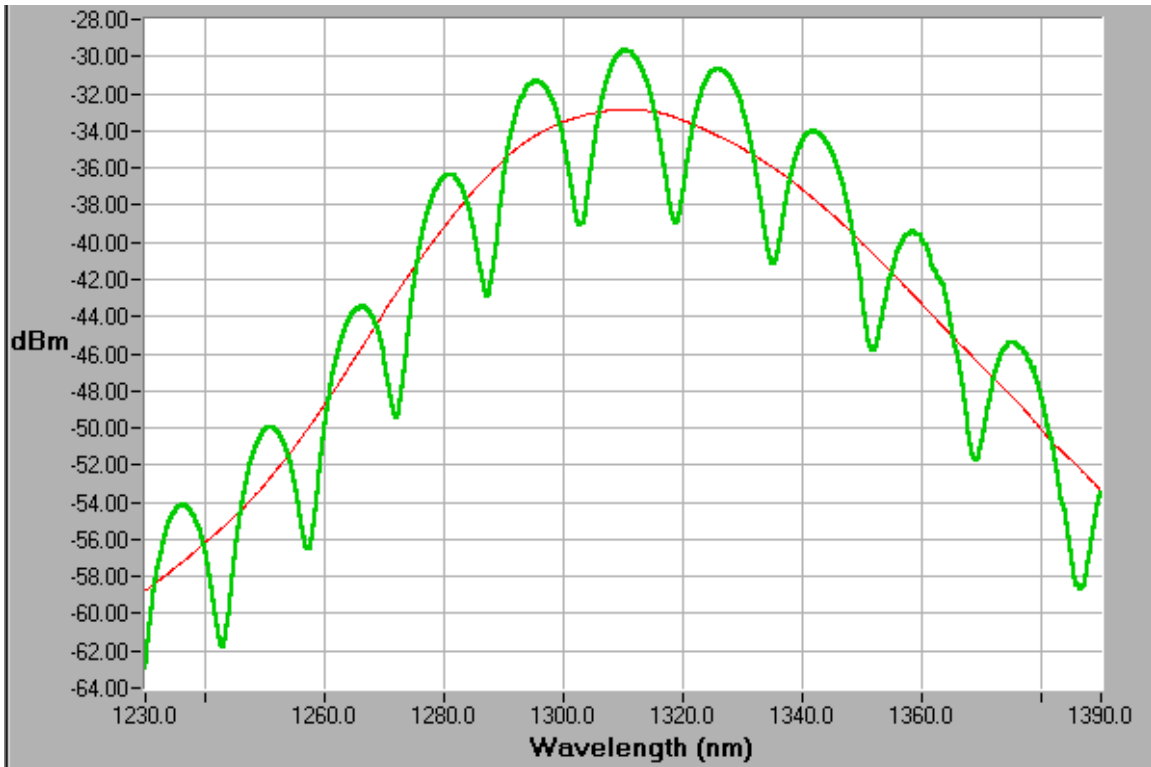
Figure 2.5 – Interference Spectrum of Fabry-Perot Sensor and Source

From the spectrum the air-gap can be directly found using the equation,

$$L = \frac{\Delta\phi\lambda_1\lambda_2}{4\pi(\lambda_2 - \lambda_1)} \qquad (2.2)$$

where L is the air-gap length, $\lambda_1$ and $\lambda_2$ are wavelengths with a phase difference of $\Delta\varphi$. Selecting two consecutive peaks from the interference spectrum sets $\Delta\varphi$ to $2\pi$, because total constructive interference only occurs at a phase difference of $2\pi$. The convenience of knowing the phase difference makes the EFPI an easily operated strain sensor[13].

## 2.4.1 Gauge Length of Extrinsic Fabry-Perot Sensors

For this experiment, a $CO_2$ laser bonded the capillary tube and fiber of the sensors and set the gauge length as the distance between the bonding points. Since the strain being transferred to the sensor is a ratio, L of Equation 1.1 is the gauge length, and the change in air-gap is $\Delta L$. Therefore an increase in the gauge length, L, will result in a greater change in air-gap length, $\Delta L$, for a given strain and vice versa. Hence, a longer gauge

length yields a more sensitive sensor.  This gives the EFPI the ability to be customized to the application.  However, a long gauge length also is more susceptible to thermal expansion and other forms of noise that can decrease its stability[13].

## 2.4.2 Strain On An Extrinsic Fabry-Perot Sensor

An easy way to strain a fiber sensor is by hanging weights from the reflecting fiber end. Figure 2.6 shows a schematic of a typical setup.
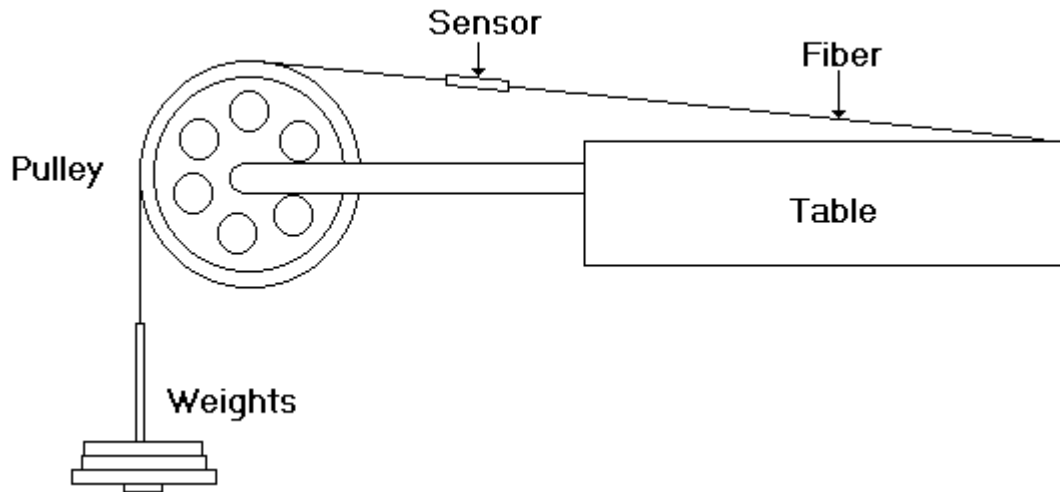
Figure 2.6 - Diagram of Strain Weight Setup.

To derive the theoretical equation for the amount of strain on the sensor we start with Young's Modulus,

$$E = \frac{Stress}{Strain} = \frac{\sigma}{\varepsilon} \qquad (2.3)$$

The Stress on a material is defined as force over area,

$$\sigma = \frac{F}{A} \qquad (2.4)$$

The force in our case is the mass times the acceleration of gravity

$$F = mg \qquad (2.5)$$

The area refers to the cross sectional area of the capillary tube that encloses the sensor or,

$$A = \pi(R_1^2 - R_2^2)$$
(2.6)

where $R_1$ is the outer diameter of the tube and $R_2$ is the inner diameter.

Substituting back into Equation 2.3 and solving for the strain provides the following equation[14],

$$\varepsilon = \frac{gm}{E\pi(R_1^2 - R_2^2)}$$
(2.7)

# Chapter 3: Multiplexing and Fourier Analysis

## 3.1 Multiplexing

Multiplexing is when information from two or more signals is put together and passed through a medium, or channel simultaneously.  The information can be either digital or analog. The three main ways to multiplex information are time, wavelength, and codes. This experiment is attempting to use Fourier analysis, a form of wavelength division multiplexing, to demodulate the interference spectrum.  Previous work by Taplin and Jackson showed demodulation of the spectrum using Fourier analysis for two Fabry-Perot cavities[15].  This research plans to expand the number of sensors to four and also provide strain measurements and comparisons as well as stability and crosstalk data.

## 3.1.1 Time Division Multiplexing

In fiber optic communications Time Division Multiplexing (TDM) is achieved by dividing the spectrum into repeating time slots.  The number of repeated time slots, N, makes a frame.  Each user or source is broken apart and only transmitted on its specific time.  This is called the buffer and burst method and requires digital modulation[16].  Since the time slots are very narrow the data stream seems uninterrupted.  An optical system first splits a continuous pulse train into the required amount of channels needed.   Each channel then has its own modulator to encode the zeroes for the data on that channel. Before the channels are multiplexed, they travel through different lengths of fiber to add a delay. The time delay is equal to one time slot, and therefore the channels are time multiplexed when they are recombined[17].

There are several ways to de-multiplex at the receiver. Some use electro-optical modulators while others make use of non-linear optics.  The similarity is that all require some sort of frame synchronization or clock signal.  The clock signal can be electrical or

an optical pulse train as in an all-optical de-multiplexer. The signal is first split up into the number of channels, and then each channel uses the clock to select out the desired data, while the rest is dumped[17].

To time multiplex sensors an optical time domain reflectometer (OTDR) provides a simple solution. An OTDR sends out a pulse and uses a fibers natural Rayleigh scattering or backscattering property to measure attenuation. The OTDR plots the intensity of the returned scattered signal as a function of distance. When the fiber is perturbed, excess loss will show up on the plot as a change in the slope of the line at the sensing distance[9], as shown in Figure 3.1.
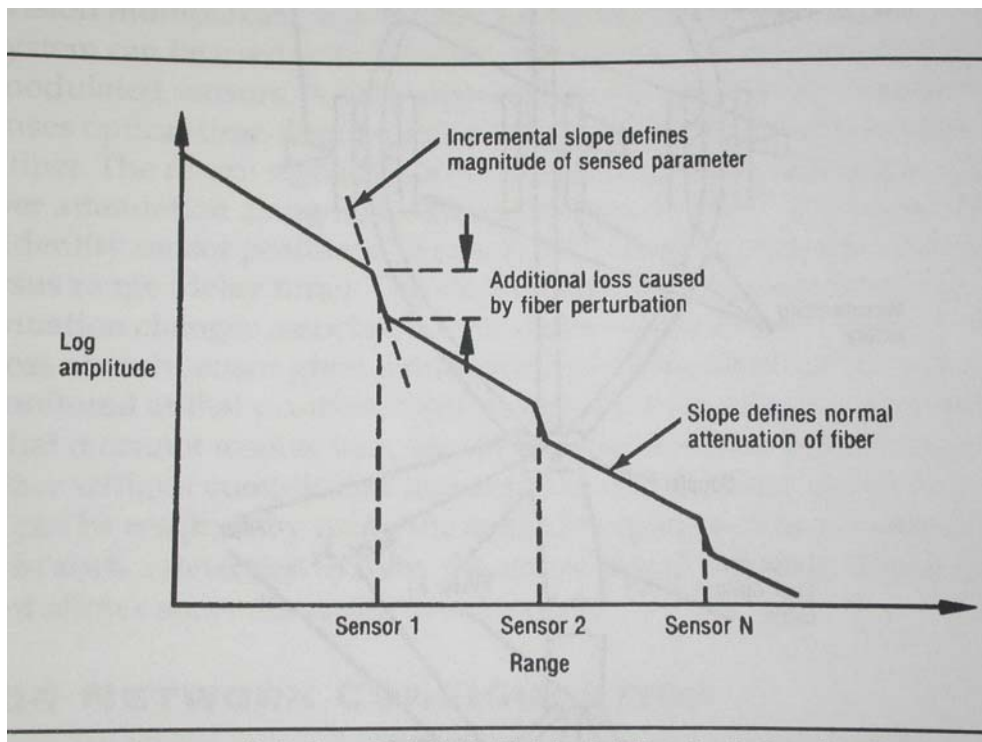


Figure 3.1 – OTDR Plot for Intensity Based Time Multiplexed Sensors[9].

Fiber Bragg gratings can also be multiplexed in time by using a star coupler to divide the source into several arms of fiber. Each arm of fiber has a loop of fiber preceding a number of Bragg gratings. Each loop has a different length and hence adds a different

time delay to each arm of sensors.  The sensing data is then retrieved in a way similar to communications data[9].

TDMA's main advantage is that it is a simple system that can be used with almost all fiber sensors. However a disadvantage is that some non-linear components for de-multiplexing are very costly, and the process can be inefficient.  Also in the OTDR system short distances cannot be resolved without expensive equipment.

## 3.1.2 Wavelength Division Multiplexing

In Wavelength Division Multiplexing (WDM) the spectrum is divided into several different bands that have their own unique frequencies.  Fiber optic systems predominately use WDM because of the amount of bandwidth available.  The low loss areas of the spectrum are at 1.3 microns and 1.55 microns with bandwidths of 12 THz and 15 THz respectively. The total capacity of the system is derived from the channel spacing.  The minimum channel spacing is at least 4 times the bit rate of the system. With the bandwidth of each channel between 40 – 50 GHz, than the potential for terabit systems becomes a reality[17].

A lot of factors can limit the use of the complete spectrum available.  Obviously very tight filtering must be done to separate the channels at the receiving end.  Also, the signals must be amplified in the case of remote sensing.  Most systems now use optical amplifiers instead of electric, and hence the bandwidth is then limited to the bandwidth of the amplifiers.  Other factors limiting the capacity are the stability of lasers, non-linear effects, and interchannel crosstalk[17].

Multiplexing of fiber Bragg gratings is an example of WDM for sensing applications. Each Bragg grating has a different index period written on the fiber, and hence reflects a different portion of the source spectrum.  Figure 3.2 shows Bragg gratings wavelength multiplexed (a) and both time and wavelength multiplexed (b) and (c).
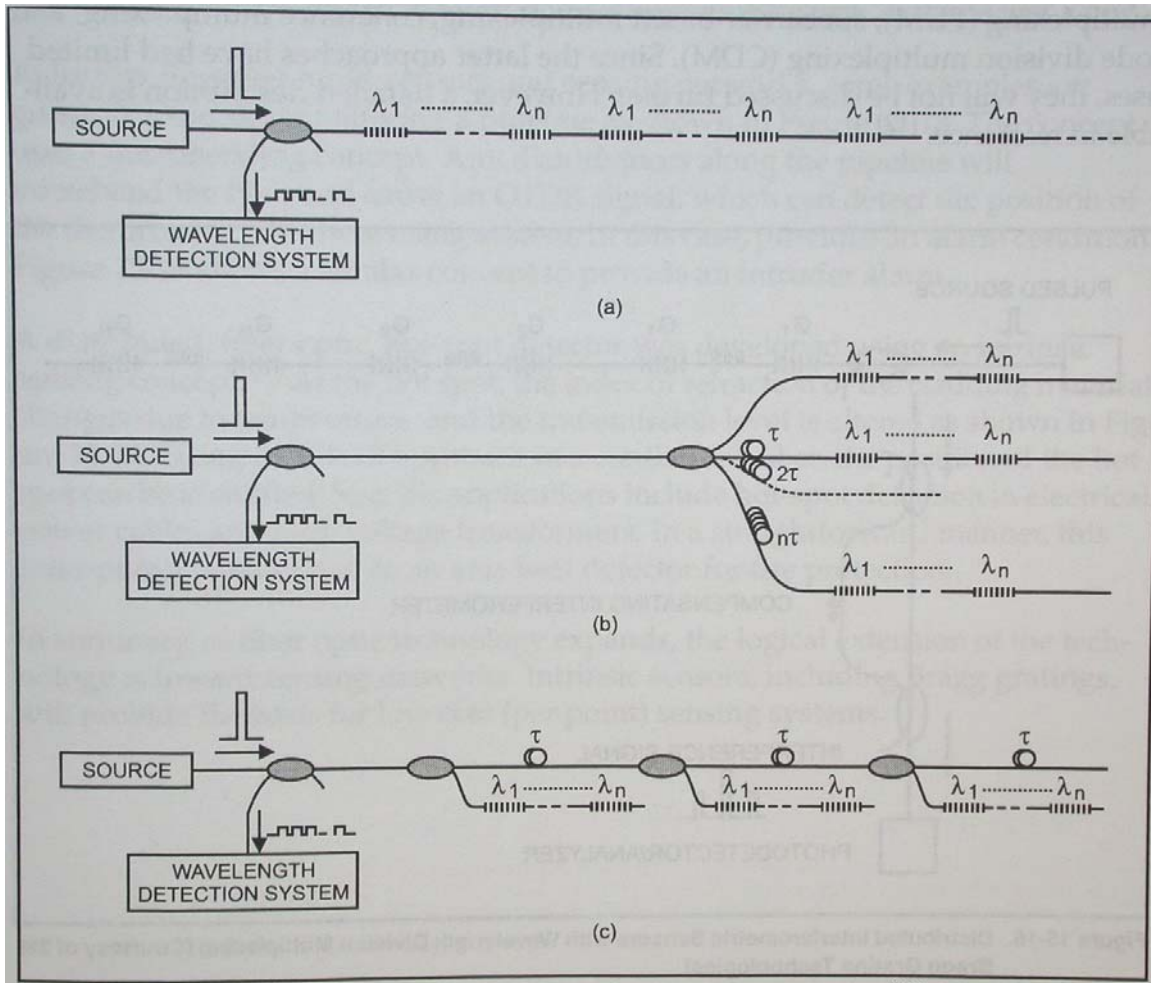
Figure 3.2 Bragg Gratings Wavelength Multiplexed (a) and Time and Wavelength Multiplexed (b) and (c)[9]

## 3.1.3 Code Division Multiplexing

So far the FDM and TDM have shown very rigid rules about allocating spectrum and time. However, with a random amount of bandwidth demand, some bandwidth can be wasted. CDM fixes the problem by using the spread-spectrum technique. The spread spectrum technique allows access to any frequency channel at any time, and is thus more efficient and flexible[17]. CDM is able to accomplish this by using codes to separate the different signals. There are a few types of coding that can be used, but first the data to be transmitted is multiplied by a spreading signal. The spreading signal is of orders of magnitude greater than the data and is usually a pseudo-noise code[16].

The first type of coding is direct sequence coding. In direct sequence coding, the data is preceded by a seven-bit code word[17] that is assumed random and orthogonal to all other code words. The receiver decodes the message using time correlation but it must know the specific codeword or the signal will appear as noise[16].

Another form of CDM is frequency hopping or hybrid spread spectrum technique. The bandwidth of the channel is divided up into smaller sections and a code is used to select which sub-band the data will be transmitted in. Each bit represents a time slot and the value of the bit represents which frequency will be used for transmission. In an optical transmission system a tunable laser can be used to accomplish the hopping.

An example of a CDM system used for multiplexing interferometric fiber sensors is using a pseudo-random code to modulate a laser source. The return pulses from each sensor have a time delay, and are demodulated by correlation with a delayed pseudo-random code[18].

Code division multiplexing in general has several advantages and disadvantages. The first advantage is that the bandwidth of a channel is more efficiently used. A higher degree of security also comes with CDM because of the random codes used to send data. CDM has a soft capacity limit and therefore has no absolute number of users. A disadvantage is the codes are not perfectly random and some self-jamming can occur from cross correlation. Also the bit error rate can be high (greater than $10^{-6}$) compared to other systems[17].

## 3.2 Fourier Analysis

Fourier analysis takes a waveform and finds any sinusoidal component imbedded in it. Using the equation,

$$W(f) = \int_{-\infty}^{\infty} w(t) \cdot e^{-j\omega t} dt \qquad (3.1)$$

one can quickly scan through all frequencies and find the ones that contribute to the waveform. An important property of sinusoids is their superposition ability. The addition of two sinusoids with equal amplitudes will yield two large values at their corresponding frequencies in a Fourier spectrum. Hence a demodulation of two signals can occur. In an optical system, reflections from two or more sensors will add to form one spectrum that is a superposition of the many[19]. This property of superposition is the most important aspect of demodulation using Fourier analysis.

## 3.3 Simulation of Data

Demodulating an optical spectrum to resolve the air-gaps of several sensors can be very difficult without some clever signal processing. Fortunately Fourier analysis can be used. As explained in the Fabry-Perot section on fiber optic sensors, a unique interference spectrum is reflected from a unique air-gap. Once the source is mathematically subtracted out, the spectrum looks very sinusoidal, but chirped. The distance between peaks at lower wavelengths is shorter than at longer ones. The theoretical sinusoid that represents the interference spectrum is given as

$$w(\lambda) = Cos\left(\frac{4\pi}{\lambda}d\right)$$

(3.2)

where d is the length of the air-gap, and $\lambda$ is the wavelength[20]. A plot of this function is shown in Figure 3.3.
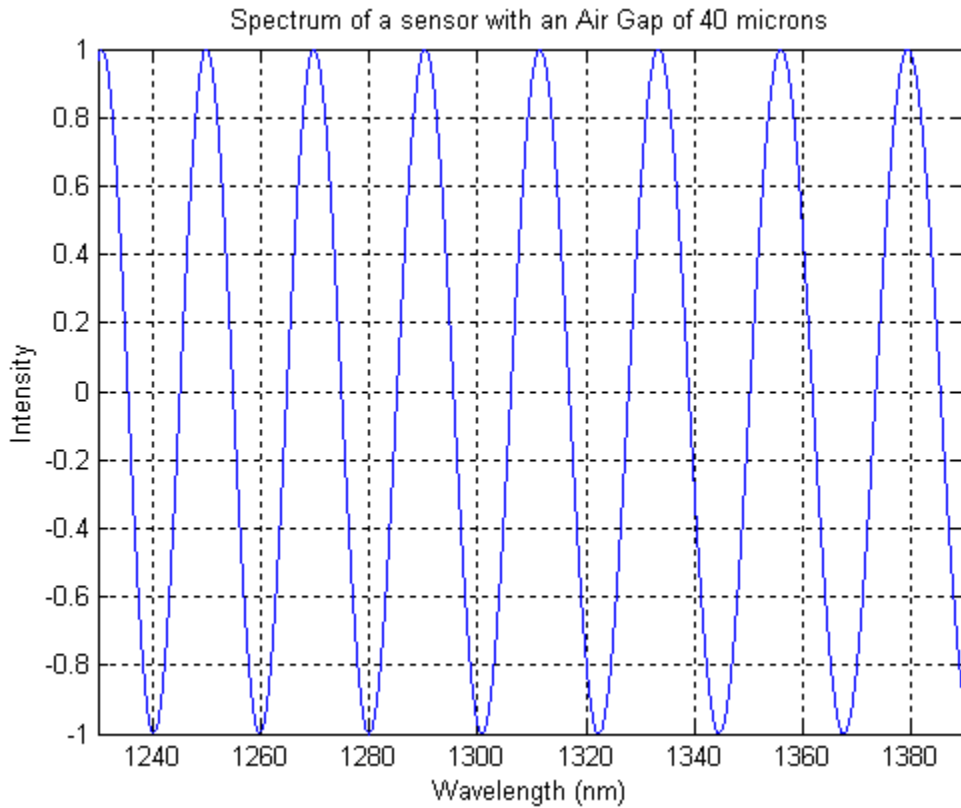
Figure 3.3 – Simulated Interference Spectrum of Fabry-Perot Sensor

One can see the chirp of the spectrum by looking at the troughs at the bottom of the graph. A direct Fourier transform of this waveform does not yield a clean peak at one frequency. In order to make this function more periodic and have a better Fourier transform spectrum, the inverse wavelength term is isolated. One can now see in Figure 3.4 the interference spectrum is periodic when Equation 3.2 is plotted against the inverse wavelength.
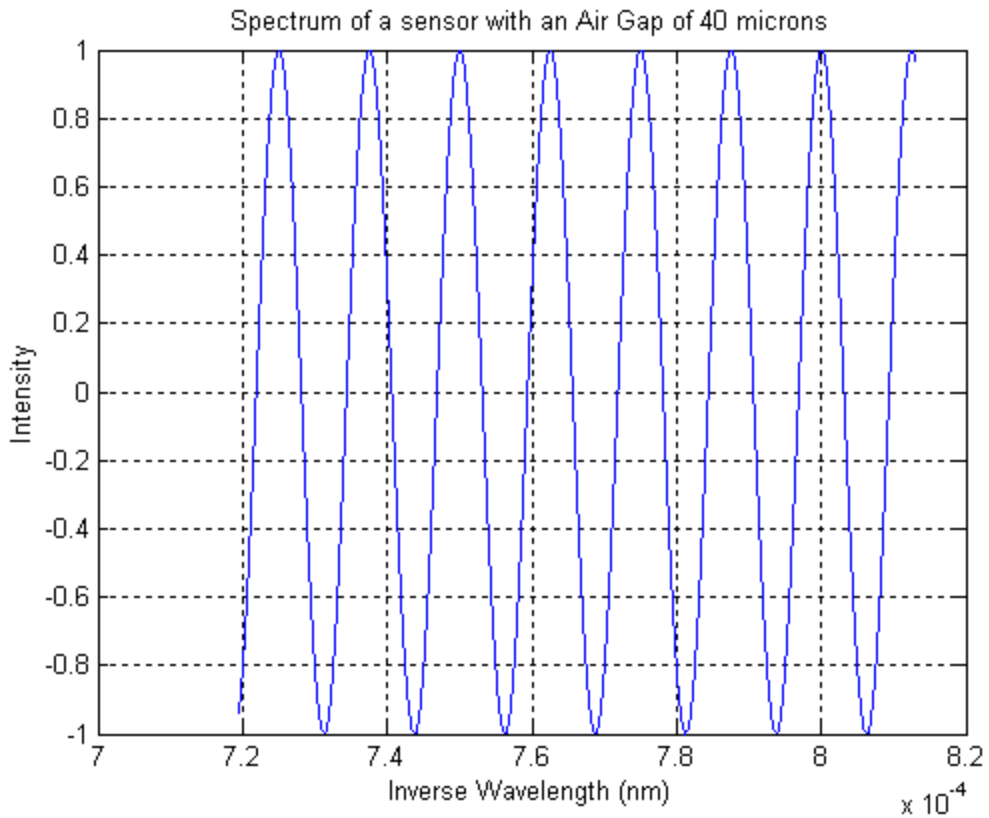
Figure 3.4 – Simulated Fabry-Perot Interference Spectrum vs. Inverse wavelength.

To get a higher sensitivity the data is zero padded to $2^{16}$ data points before the Fourier transform is taken. For each unique air-gap, or spectrum, a unique Fourier peak is found. Figure 3.5 shows an example.
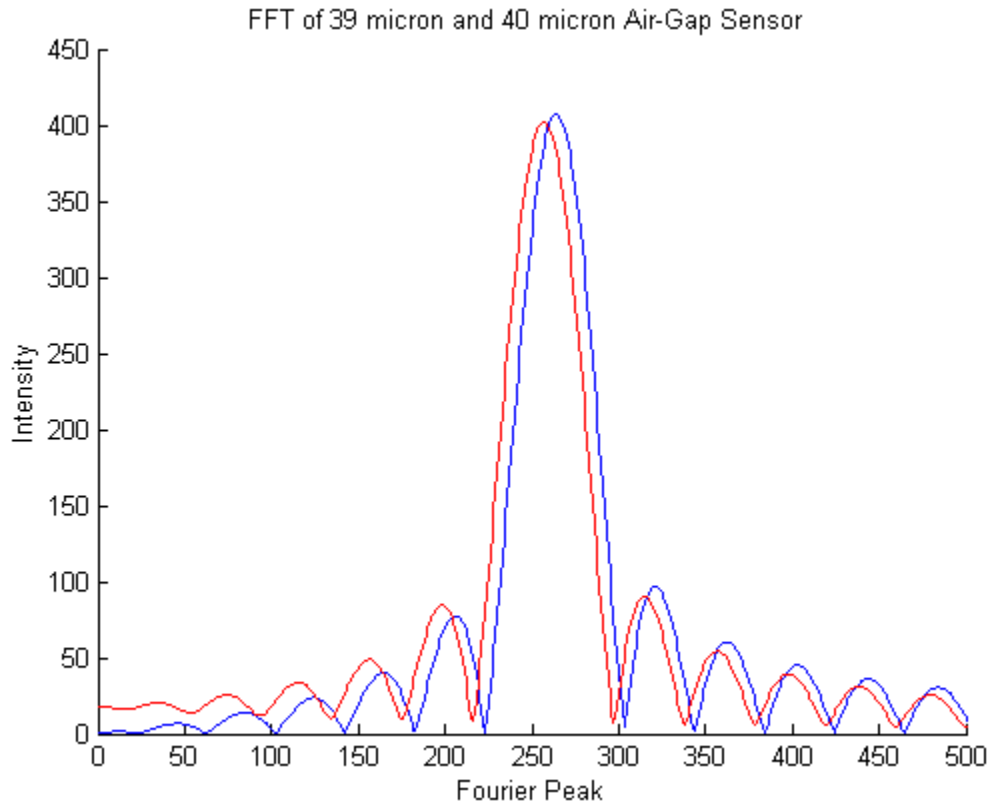
Figure 3.5 – Fourier Transform of Simulated 39μm and 40μm Interference Spectrum.

As the air-gap increases the Fourier peak position will shift to higher values, simply because a larger air-gap sensor has a greater number of oscillations on the interference pattern. The reverse is also true, as the air-gap decreases the Fourier peak position will decrease. There is a linear trend between the FFT peak position and the air-gap. Figure 3.6 shows the air-gap as a function of Fourier transform peak.

**FFT to Air Gap Conversion**
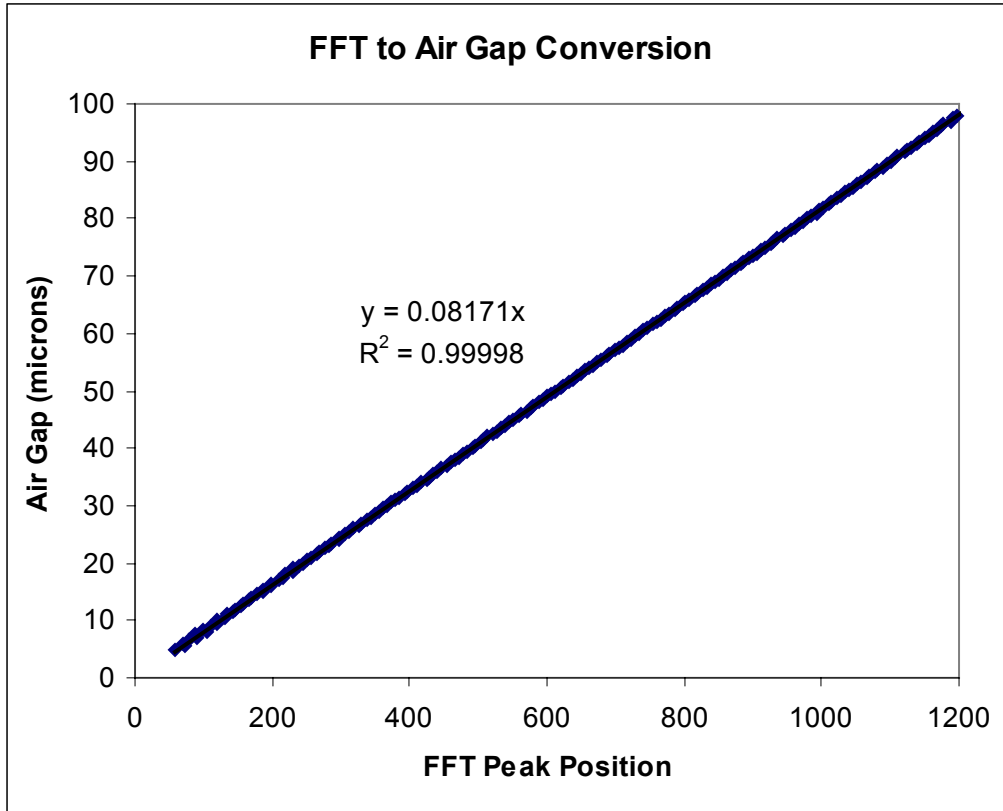


$y = 0.08171x$
$R^2 = 0.99998$

Figure 3.6 – Simulated Air-Gap vs. Fourier Peak

The slope of the line represents the conversion factor for the system. It also represents the maximum sensitivity of the system. There is a direct relationship between the amount of points in the data set and the ultimate sensitivity of the system. Doubling the amount of data doubles the sensitivity. For example the current sensitivity is 0.08171 microns, or the slope of the conversion line. If the zero padding were increased so there was $2^{17}$ points, the sensitivity would be 0.0485 microns. However more data points also increases the computation time of the computer, and $2^{16}$ points was a good balance between sensitivity and computation time.

## 3.4 Stability and Crosstalk In A Multiplexed System

A drawback to any multiplexed system is its stability and crosstalk. The stability is the standard deviation of the air-gap while there is no change in strain. Theoretically no strain would imply no change in air-gap and a standard deviation of zero. However,

every system has noise, some from outside and some from inside.  Outside vibrations and temperature fluctuations can cause instability.  Inside, the spectrum is zero-padded and a Fourier transform is taken, where slight fluctuations can significantly change things.

The crosstalk is the stability of all the sensors while one or more is being strained.  The main cause of crosstalk is from the sidelobes and harmonics from other sensor's Fourier peaks.  Each sensor's peak has sidelobes that stretch over the entire spectrum.  These sidelobes interfere with the peaks of other sensors because as the peak for the strained sensor moves, the sidelobes move too and can cause slight fluctuations in the peaks of other sensors.  One can easily see the sidelobes in Figure 3.5.

To reduce the crosstalk between sensors Equation 3.2 was used to simulate a spectrum at the gap of the sensor being strained.  The resulting spectrum was then zero padded and the Fourier transform was taken.  The sidelobes from the simulated spectrum were subtracted from the actual experimental spectrum.  Figure 3.7 shows only the sidelobes for a sensor with an air-gap of 35 microns.
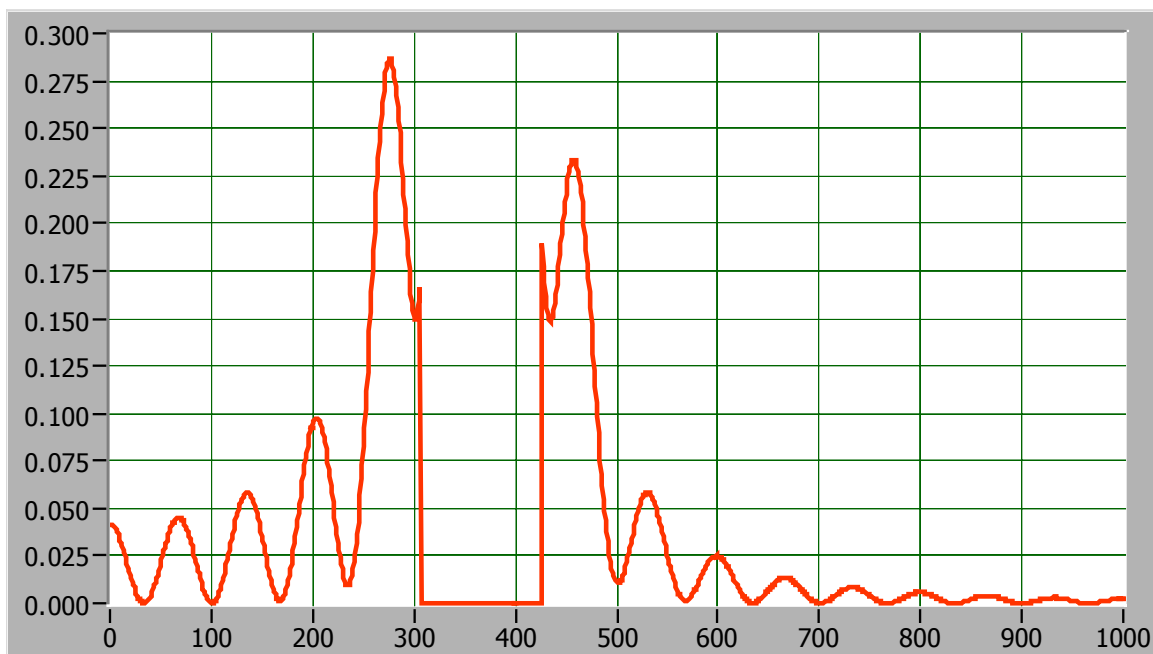


Figure 3.7 – Subtracted Sidelobes of 35 micron Air-Gap Sensor

# Chapter 4: Experimental Setup and Results

## 4.1 Basic Setup

The following experiment was designed to test the feasibility of a multiplexed fiber sensor system. Along with the amount of sensors that can be multiplexed, the stability and accuracy were tested as well. The extrinsic Fabry-Perot Interferometer was chosen because of its high sensitivity of air-gap measurement, and its almost independence of temperature. When many sensors are multiplexed together the power of the system is divided between them, therefore the higher the power the more sensors that can be multiplexed. Based on the availability of high power single mode fiber pigtailed light sources (1300 nm wavelength), single mode fiber was chosen for the entire system. Another benefit of the single mode fiber EFPI is the light coming out of the core of the lead fiber has a small divergence angle so large air-gap EFPIs become possible. Also, the single mode EFPI is very easy to fabricate compared to the multimode. Detection of a 1300 nm wavelength required the use of the Ando AQ-6315A Optical Spectrum Analyzer (OSA).

The conservation of power was very important and therefore a circulator was used to direct the light from the source to the sensor, and then back to the OSA with minimal loss. Also, a one by four Y-junction was used to multiplex the sensors in parallel.

De-multiplexing the sensors was a task in programming and signal processing. LabVIEW was chosen for the program to control the OSA and download the data for signal processing. Figure 4.1 shows a diagram of the experimental setup.
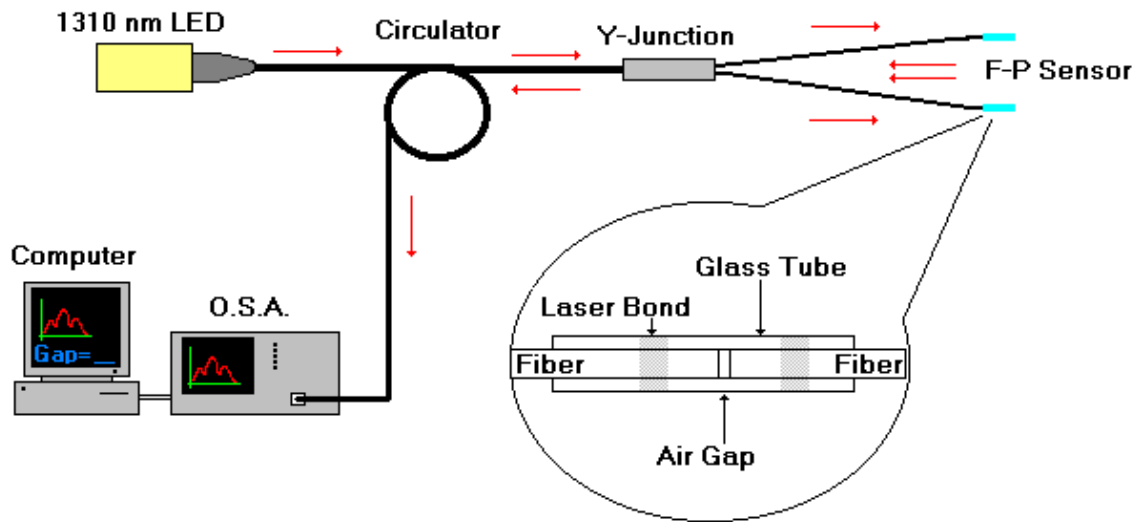
Figure 4.1 – Experimental Setup Diagram

## 4.2 Verification of Simulation

The first thing done was verifying the simulated Fourier transform peak to air-gap calculation. A special sensor that had the reflected end attached to a micrometer was spliced to the system. The sensor air-gap was then swept from approximately 13 microns to 80 microns at random intervals. At each interval the air-gap was calculated two ways and compared. The first was using Fourier analysis on the spectrum and the simulated conversion multiple to calculate the air-gap. The second was finding the spectral peaks and using Equation 2.2. A plot of the experimental versus the calculated gap is seen in Figure 4.2.
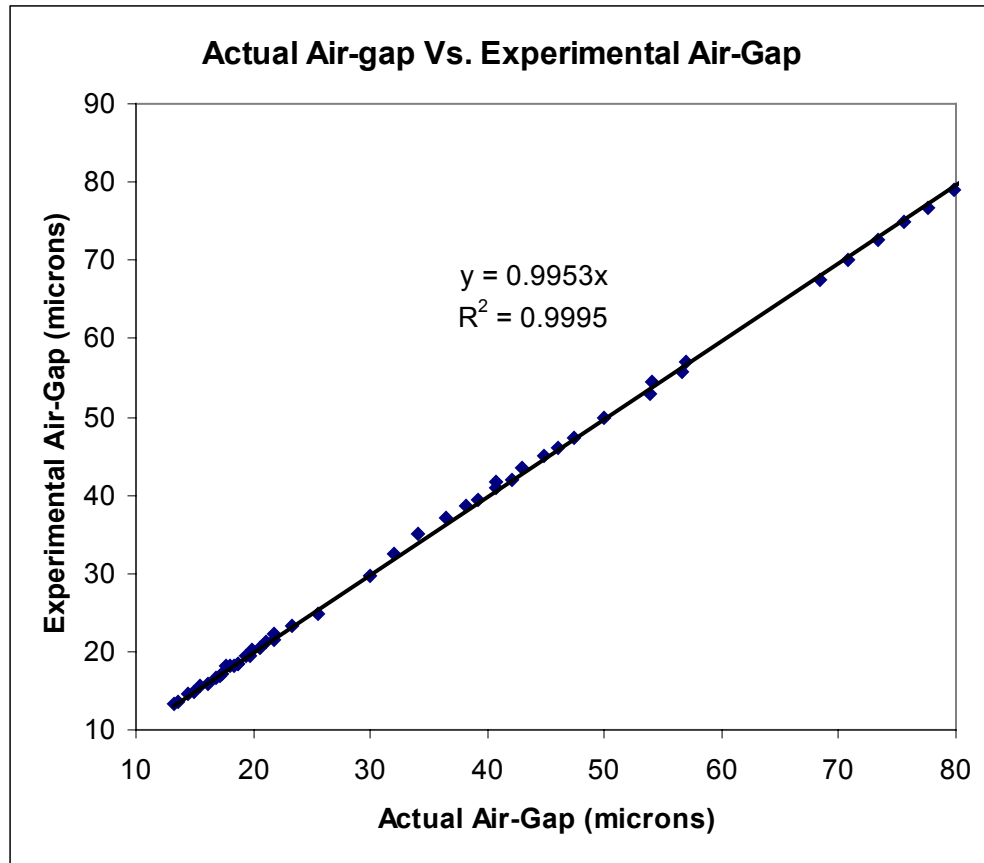
Figure 4.2 – Experimental Air-Gap Vs. Actual Air-Gap

The slope of the line and its R-squared term are very close to unity, and therefore show the simulated Fourier transform peak to air-gap conversion multiple is valid.

## 4.3 Verification of Strain Accuracy

The first method to measure the strain was the hanging weights method.  Figure 4.3 shows a picture of the setup.

Figure 4.3 – Picture of Weight Setup

A hook was attached to the reflecting fiber end of the sensor. Weights were added and the spectrum was analyzed after each weight to resolve the air-gap. Figure 4.4 is a plot of the experimental change in air-gap versus the theoretical change air-gap.
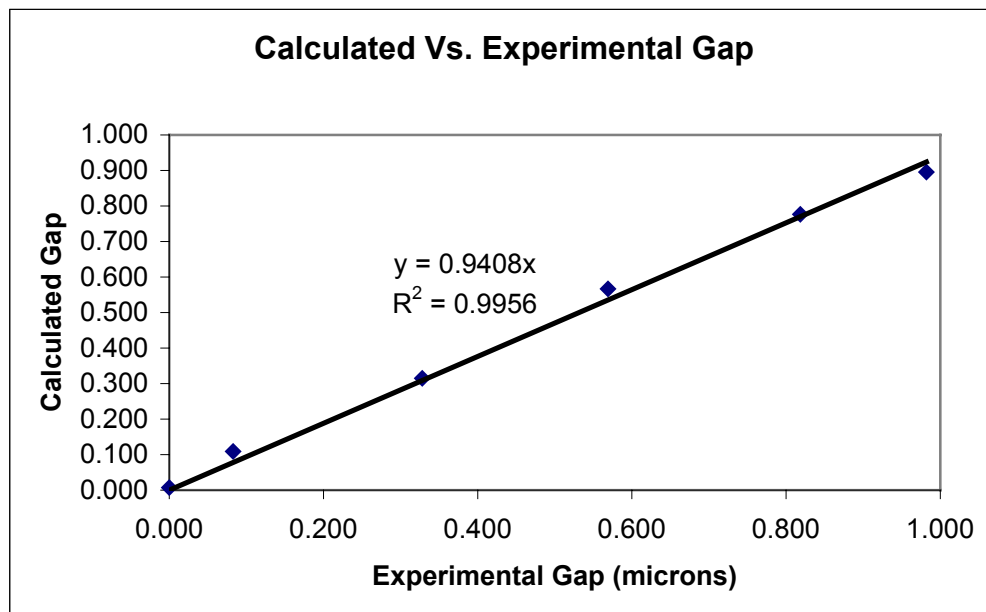


Figure 4.4 – Weight Strain Experimental Air-Gap Change vs. Theoretical Air-Gap Change

The cantilever beam method was the second method used to create strain for measurement. A rectangle was cut from an aluminum sheet to make the test piece. Sheet metal was chosen because it is thinner and can be bent easier than a bar. First the foil strain gauge was epoxied on and all the electrical connections were made. Next the fiber sensor was glued to the test piece using ordinary quick drying glue. The center of the fiber sensor actually was not in the same place as the foil strain gauge and hence they could not be compared to each other, but only to the theoretical values calculated for each spot. One end of the beam was clamped down to the table and the other displaced using a step block. Figure 4.5 is a picture of the experimental setup and Figure 4.6 shows the results.
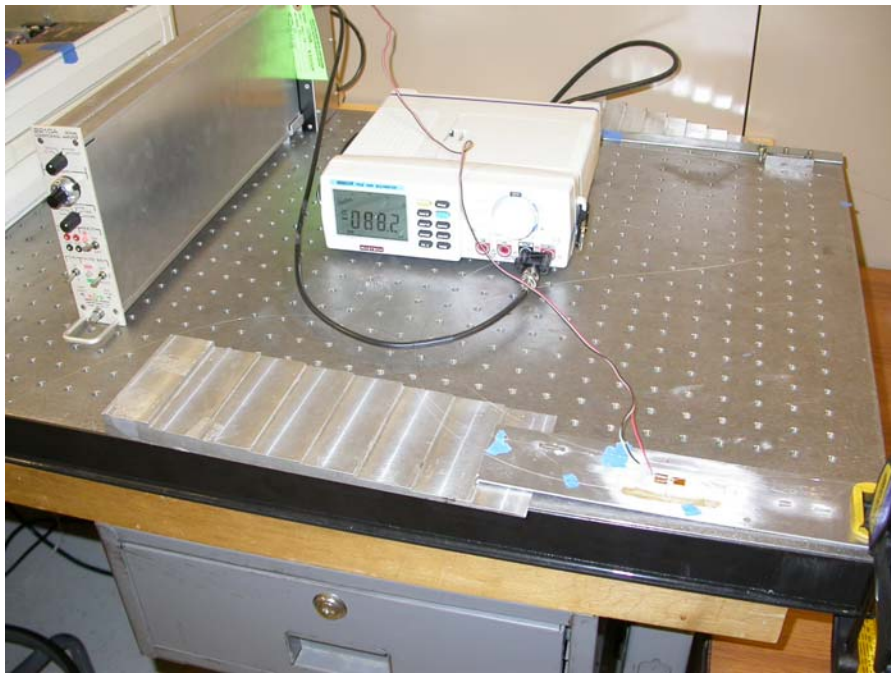


Figure 4.5 – Picture of Cantilever Beam Strain Setup

**Fiber Vs Foil Strain Accuracy**

$y = 0.994x$
$R^2 = 0.9895$

$y = 0.9713x$
$R^2 = 0.9932$

Calculated Strain (microstrain)

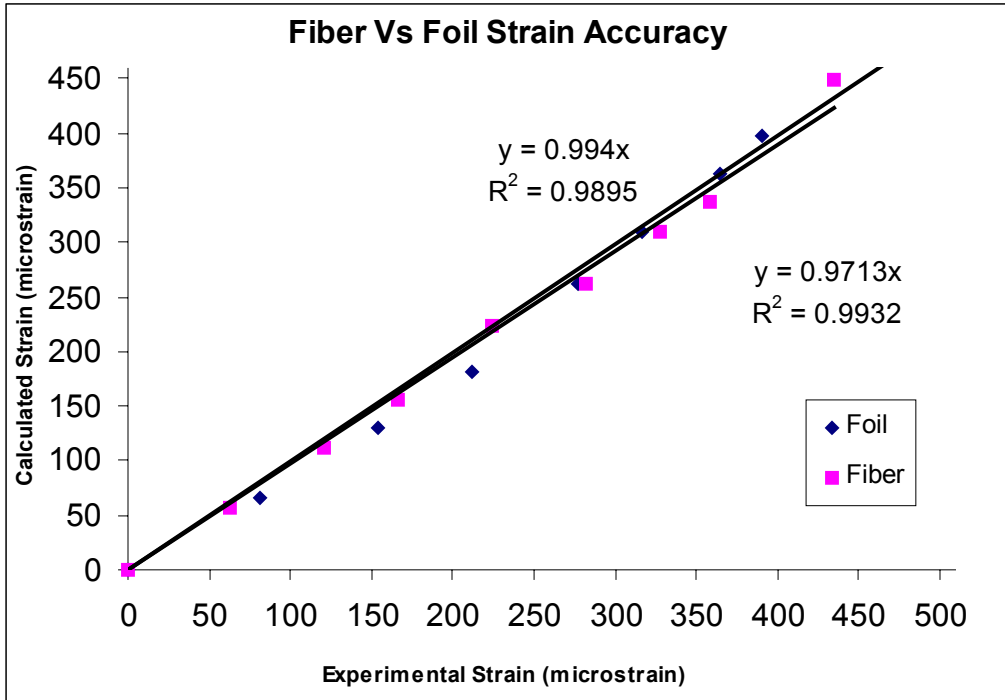Experimental Strain (microstrain)

Foil
Fiber

Figure 4.6 – Cantilever Beam Fiber and Foil Experimental Strain Vs. Theoretical Strain

One can see the agreement with theoretical values was far better in this experiment. A separate test piece with only a fiber sensor was also made. The calculated and experimental values for the change in air-gap can be seen in Figure 4.7.
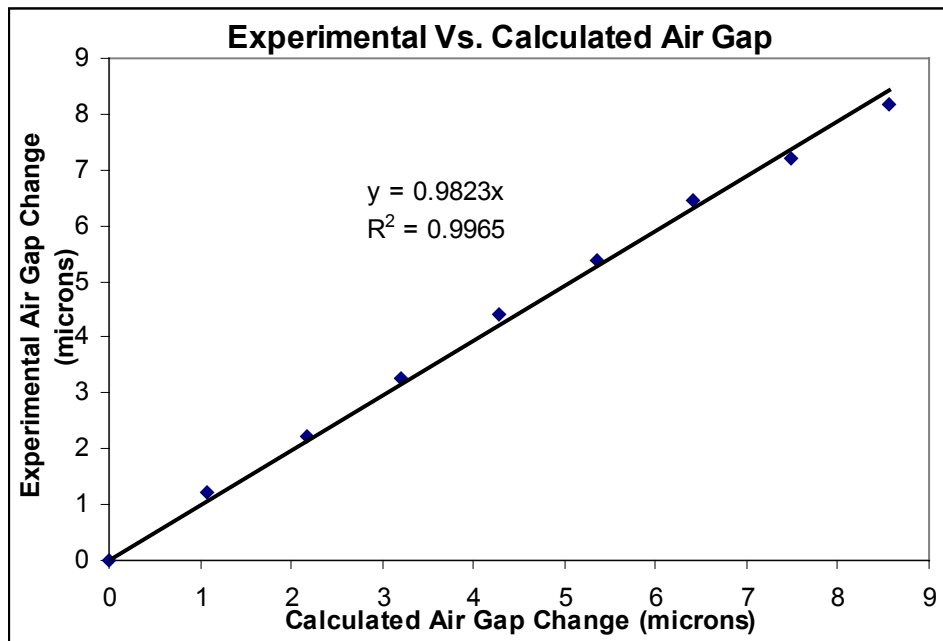


**Experimental Vs. Calculated Air Gap**

$y = 0.9823x$
$R^2 = 0.9965$

Experimental Air Gap Change (microns)

Calculated Air Gap Change (microns)

Figure 4.7 – Experimental Air-Gap Change vs. Theoretical Air-Gap Change

## 4.4 Multiplexing Two and Four Sensors

The next step was to try and multiplex two sensors.  A 3dB coupler was used to multiplex each sensor in parallel.  Each sensor's spectrum was taken individually first and then plotted over the spectrum of the two sensors multiplexed.  One can see in Figure 4.8 how the spectrum of both sensor's (green and blue) sinusoidal components add and form the multiplexed spectrum (magenta) using superposition.
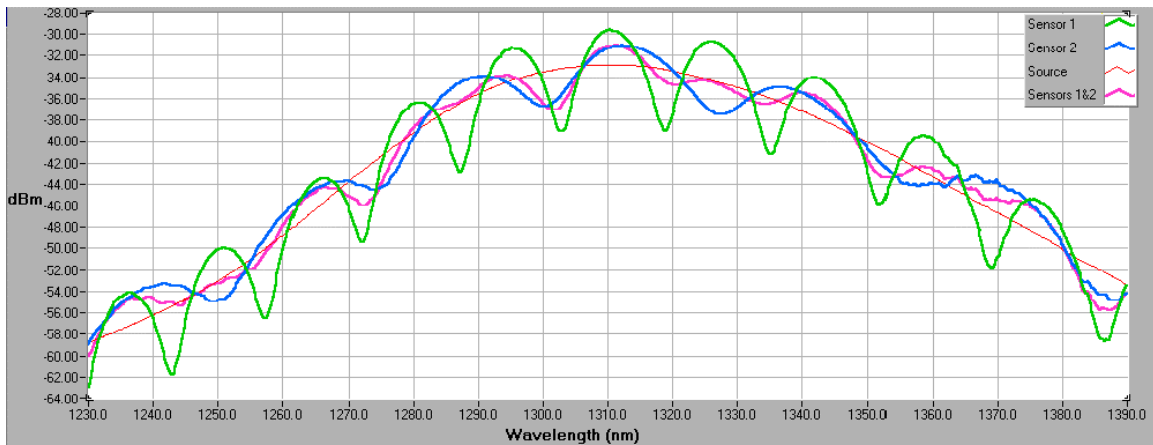


Figure 4.8 Two Multiplexed Sensor's Spectrum over Individual Spectrums and Source

Figure 4.9 shows the Fourier transforms of each individual sensor as well as the transform of the sensors combined.  It is clear the length of the air-gap for each sensor was preserved in the multiplexing de-multiplexing processes.
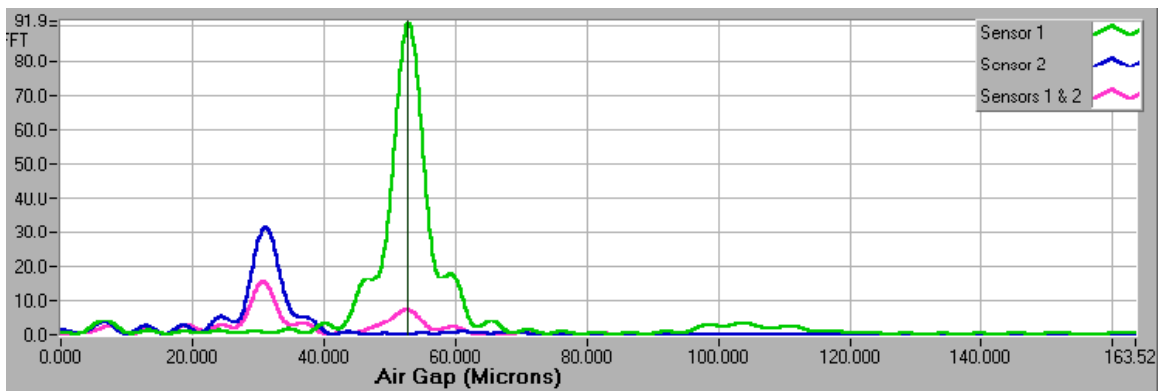


Figure 4.9 – Two Multiplexed Sensor's FFT Spectrum over Individual FFT Spectrums

To conserve power a one by four coupler was used to multiplex four sensors together. However, the traditional EFPI made only of single mode fiber did not reflect enough power back to the O.S.A., and therefore precious information was lost in noise. Applying a highly reflective coating to the end of the reflecting fiber did two things for the system. The first was increasing the amount of reflected light and therefore increasing the amount of power returned to the O.S.A. It also allowed the possibility of increasing the air-gap to over one hundred microns. The ability to make sensors in a larger range of air-gaps increases the amount of sensors that can be multiplexed. This is because each sensor has an amount of air-gap space to move around in during straining. Therefore more space leads to more sensors. More space can also lead to more reliability and stability, because there is less chance the air-gaps will interfere with each other.

The coating with the highest reflectivity is gold, and therefore exactly what was needed for the project. Once all four sensors had their coatings they were multiplexed together. In the first run the sensor with smallest air-gap reflected so much energy that it almost drowned out the sensors with very large air-gaps. Bending the fiber slightly introduced just enough loss to put the small air-gap sensor on the same power level as the others, and made the Fourier peak spectrum easier to read. Figure 4.10 shows the interference spectrum and Figure 4.11 shows the Fourier transform of the four gold coated sensors multiplexed.
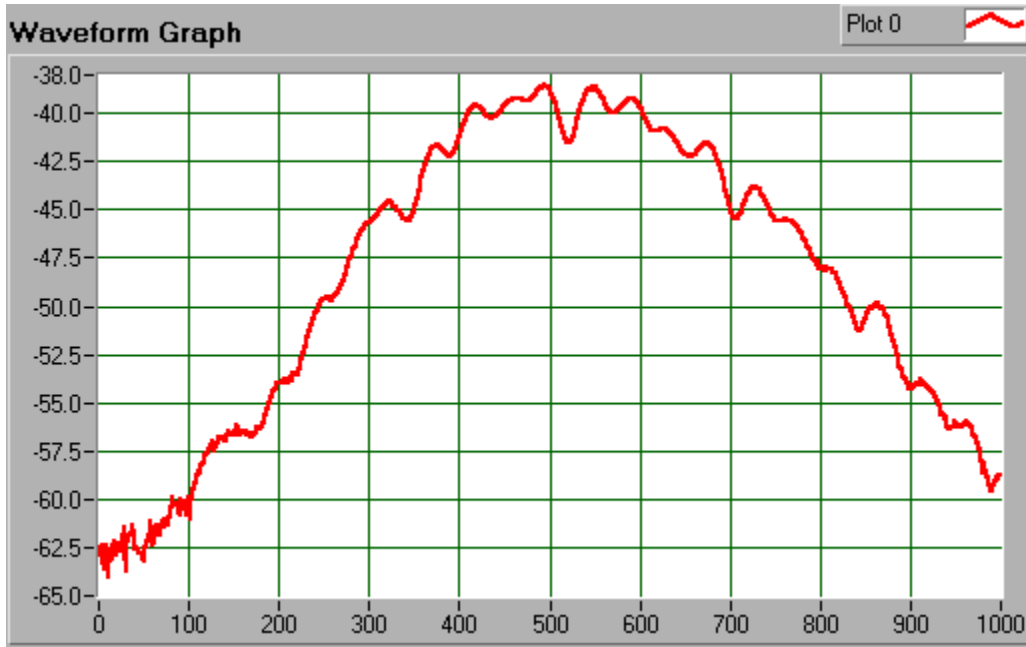
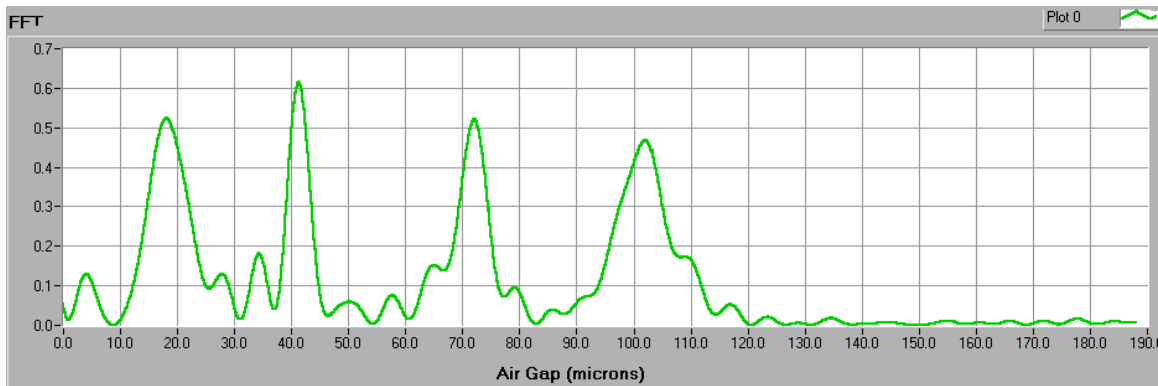Figure 4.10 – Interference Spectrum of Four Multiplexed Sensors


Figure 4.11 - FFT Spectrum of Four Multiplexed Sensors

## 4.5 Stability and Crosstalk Measurements

The stability of one, two, and four sensors was taken.  The experiment consists of splicing on one or many sensors and taking many air-gap readings without disturbing the sensors.  Figure 4.12 shows the results.
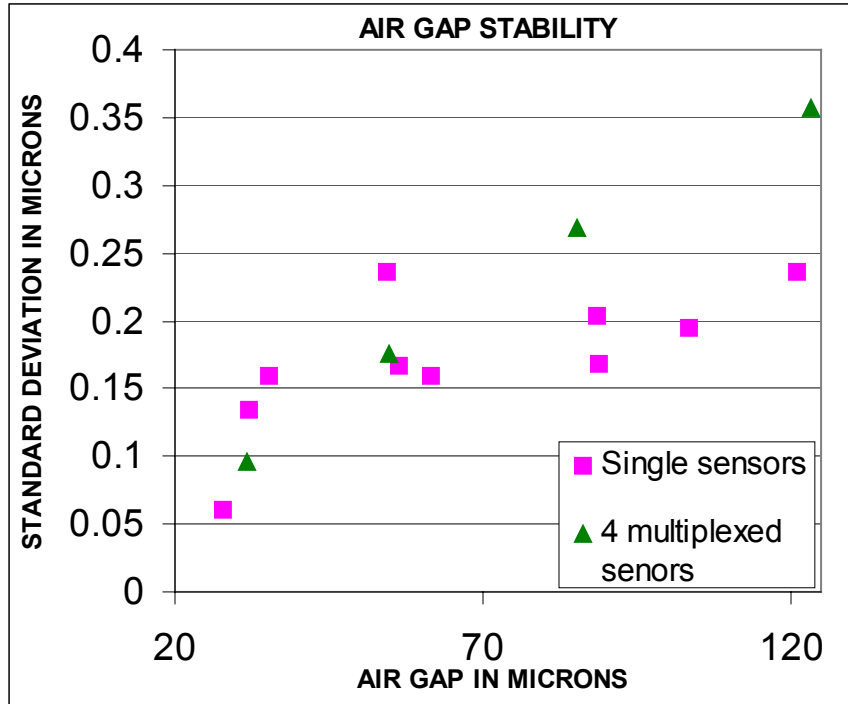
Figure 4.12 – Sensor Stability Vs. Sensor Air-Gap

Finally the crosstalk and suppression technique of the system were tested. All four sensors were multiplexed and the stability was measured. Next, the first sensor was strained and the change in the air-gap was recorded in all four sensors twice; once with no sidelobe suppression and once with sidelobe suppression. From Table 4.1 one can see the crosstalk with and without sidelobe suppression compared to the stability of the sensors.

| Sensor Gap | Stability (µm) | Standard Deviation While Sensor 1 is Strained (µm) | |
| --- | --- | --- | --- |
| | | With no Sidelobe Suppression | With Sidelobe Suppression |
| 32.002 | 0.13 | N/A | N/A |
| 55.362 | 0.21 | 0.223 | 0.213 |
| 88.154 | 0.18 | 0.414 | 0.396 |
| 115.956 | 0.65 | 0.719 | 0.659 |

Table 4.1 – Stability and Crosstalk of Four Sensors Before and After Sidelobe Suppression

# Chapter 5: Conclusions and Future Work

## 5.1 Conclusions

The feasibility to multiplex four EFPI using Fourier analysis for demodulation has been shown.  The applications of the system are vast in that demodulation yields the change in air-gap, and hence can be attached to any kind of EFPI sensor.  The following conclusions can be made from this experiment.

- Demodulation of the air-gap using Fourier analysis had an accuracy of greater than 99.5% for air-gaps ranging from 13 to 80 microns.  The error in the accuracy comes from the fact that the interference spectrum is not a perfect sinusoid.

- The system has an air-gap resolution of 0.08 microns, which corresponds to about 8 μstrain for a sensor with a gauge length of 10 mm.  The standard deviation of air-gap measurements increased as more sensors were multiplexed and as air-gap increased.

- The system showed to be 97% in line with theoretical values with an $R^2$ value of 0.9932, compared to the foil strain gauge that was within 99% of theoretical values with an $R^2$ value of 0.9895.  A separate test showed the fiber sensing system to have a 98% correlation to theoretical air-gap changes.

- The sidelobe suppression technique decreased the crosstalk in two of the three sensors to nearly zero and to a few tenths of a micron in the third sensor.

- A total of four sensors were multiplexed and demodulated with each sensor's Fourier peak occupying approximately 20 microns of space. With an air-gap of 120 microns easily attainable, multiplexing of six sensors is possible.

- Overall using Fourier analysis to demodulate the sensors air-gaps was a success. Now that the properties and tolerances of the system are known, a specific situation for application can be found.

- A drawback of the system is the O.S.A. Not only is it expensive, but also its scanning rate has a maximum of 1 Hz, which is a few orders of magnitude lower than what is acceptable.

## 5.2 Future Work

The next phase for this project is to buy a one by six multiplexer and attach six sensors. The scanning frequency is the next hurdle for this system. A detector must be developed or found that can sample the spectrum at a minimum of 100 Hz. Once these two issues are taken care of the system can be tested on a mock elevator beam setup. Tests of the fiber sensors verse electronic sensors can be compared to see if the system is accurate and stable. If possible considerations of price should become part of the final goal. After all a system that is better and around the same cost or less is ideal.

An improvement on the system that is waiting for better or cheaper technology is the source. Hopefully, future technology will bring a high-powered LED with a large bandwidth. As stated earlier, an increase in both power and bandwidth directly leads to more sensors, less crosstalk, and better stability for the Fourier demodulated multiplexed Fabry-Perot strain sensing system.
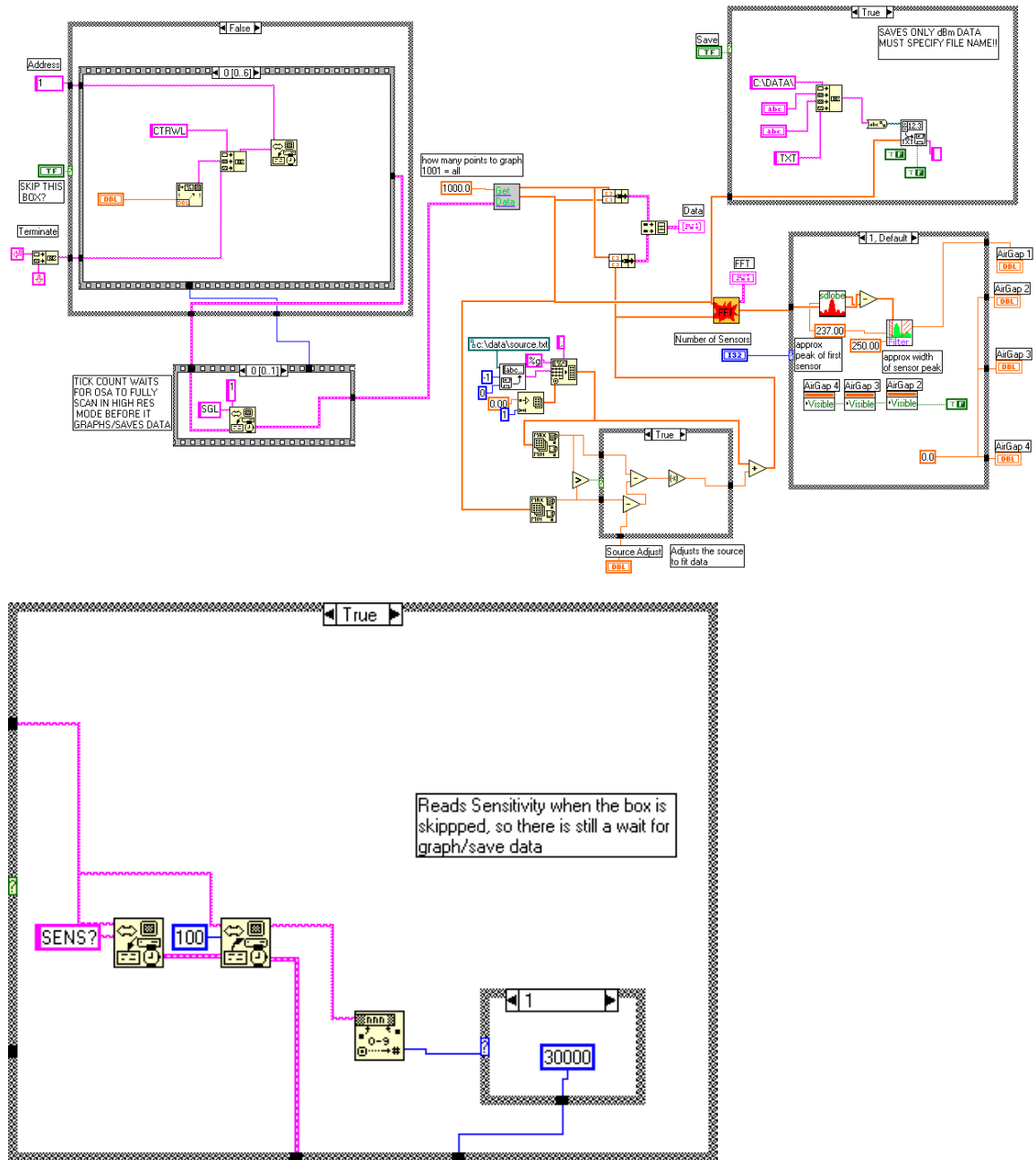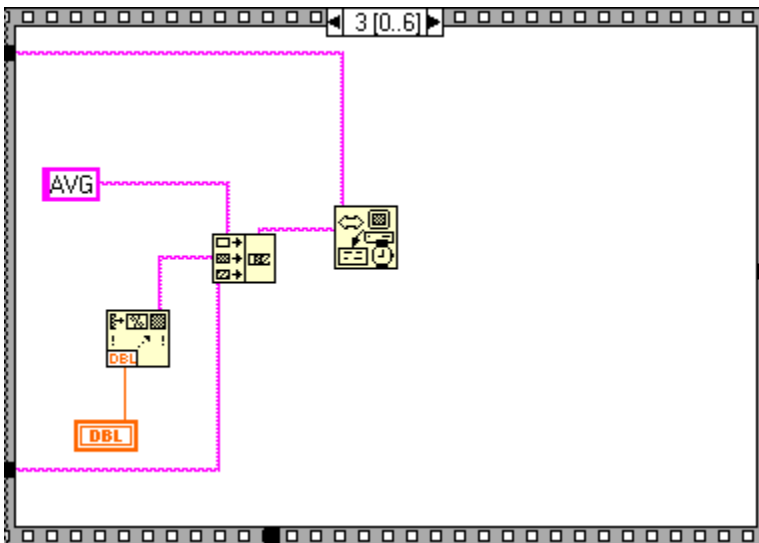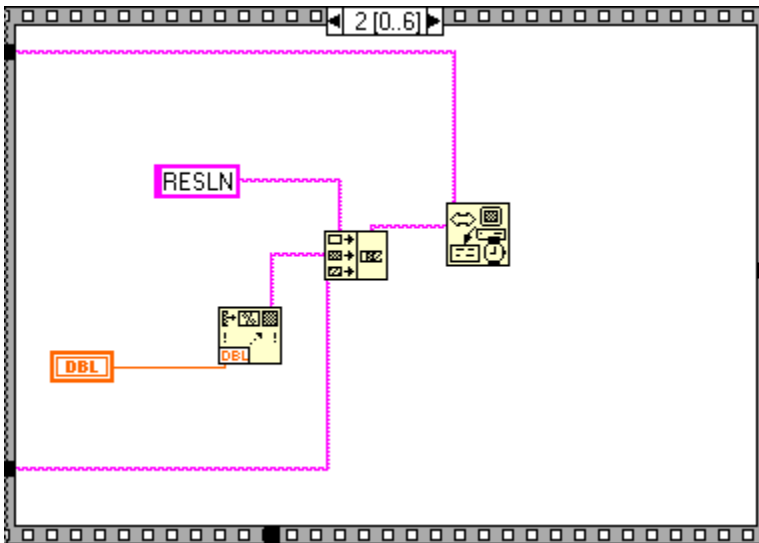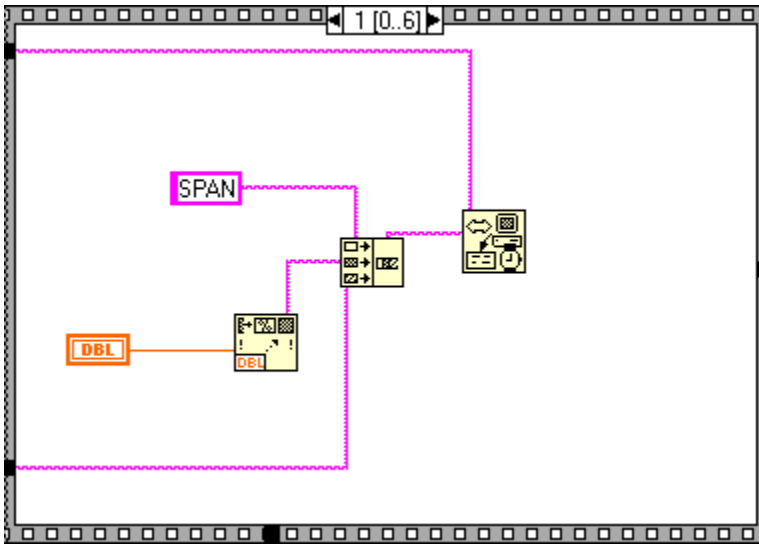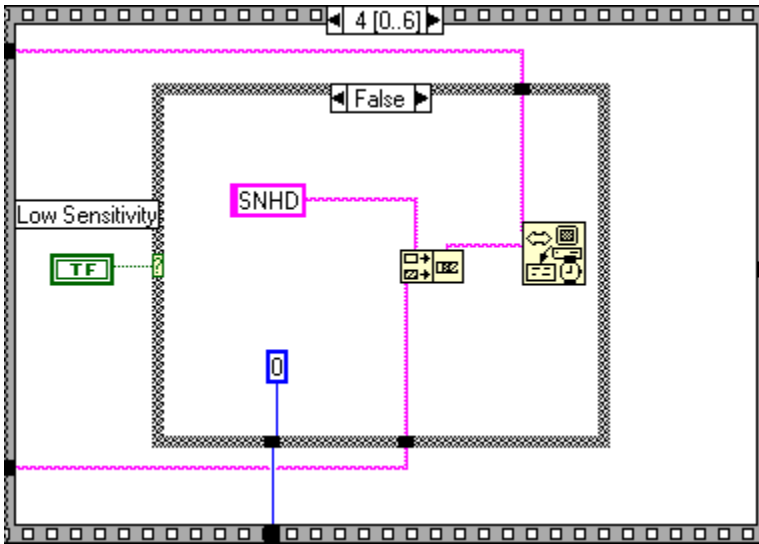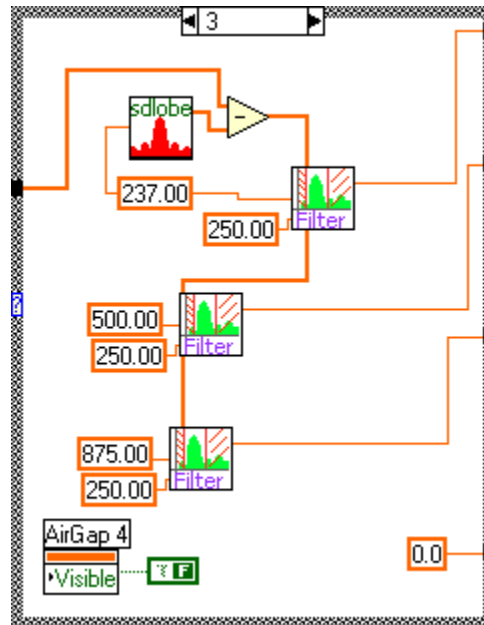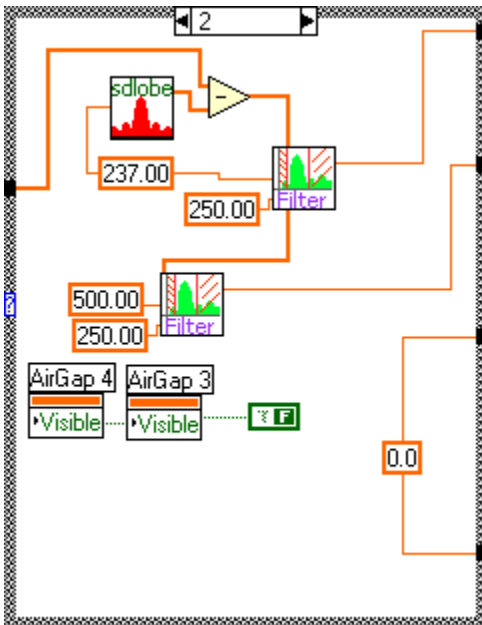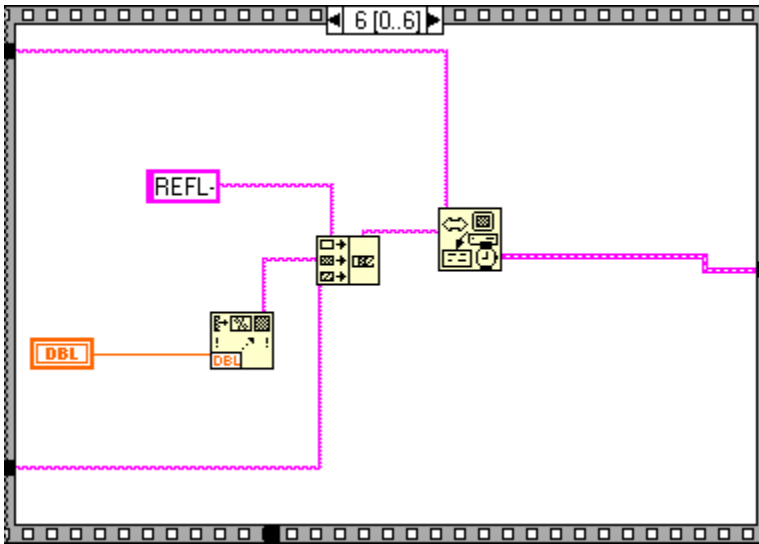
# Appendix A
LabVIEW Code

## A.1 OSA_Control.vi

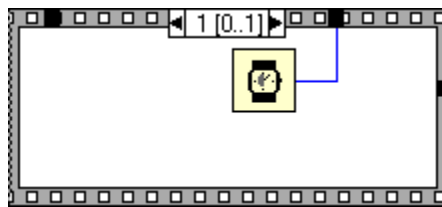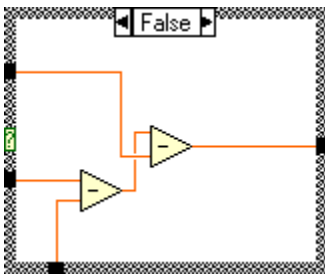The main program that controls the OSA and analyzes the data using other sub-programs.
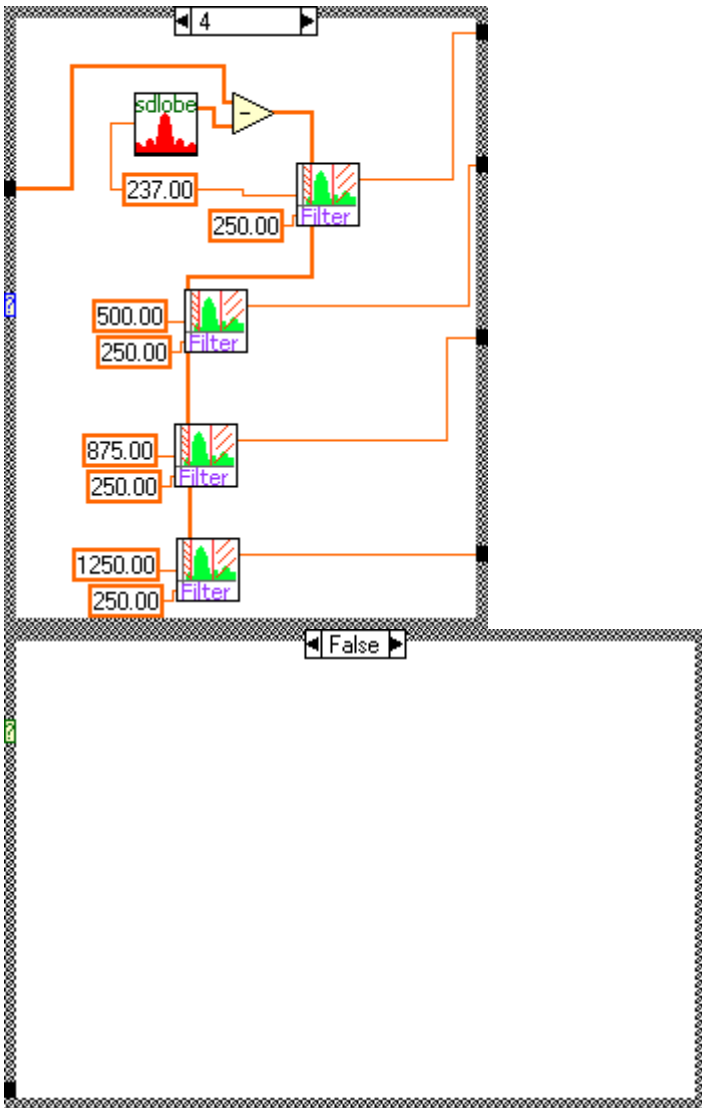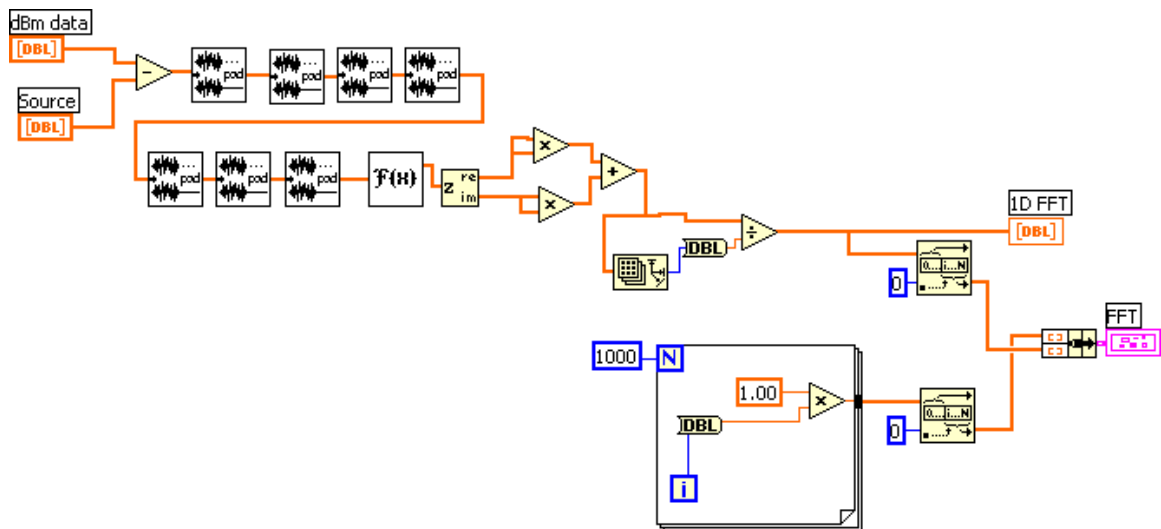
## Block Diagram
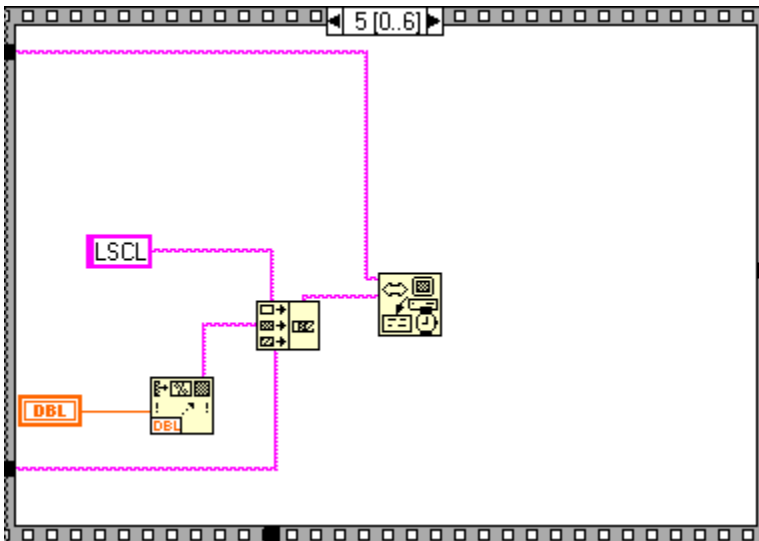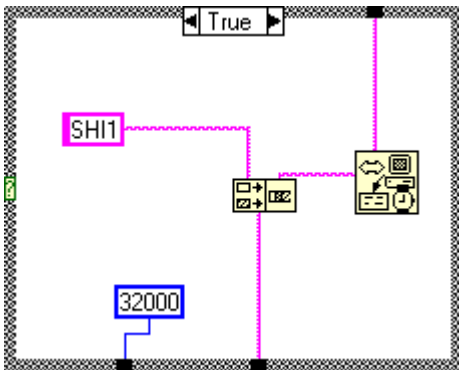
# A.2 FFT.vi

Inputs source and dBm data and zero pads to 65536 points. Takes the FFT and plots both the 1D and a 2D spectrum.

## Connector Pane



## Block Diagram



# A.3 OSADataGet.vi

Gets wavelength and dBm data from the OSA and converts it into a 1D format.

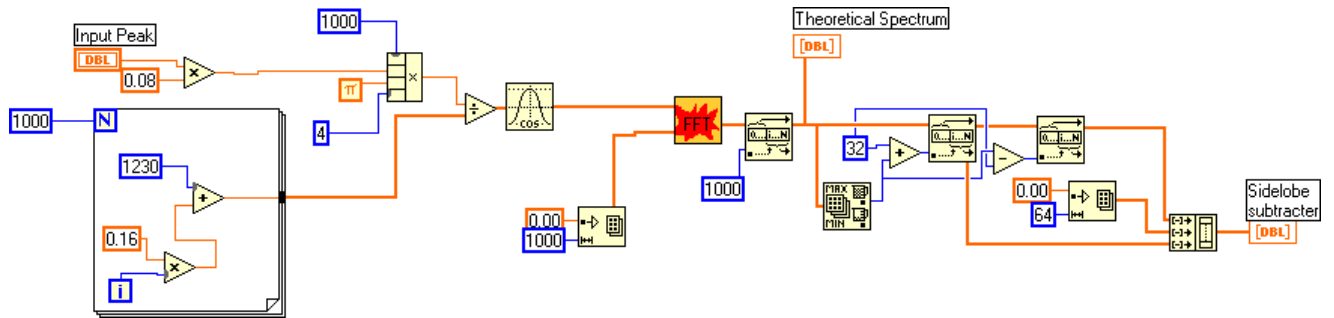## Connector Pane



## Block Diagram
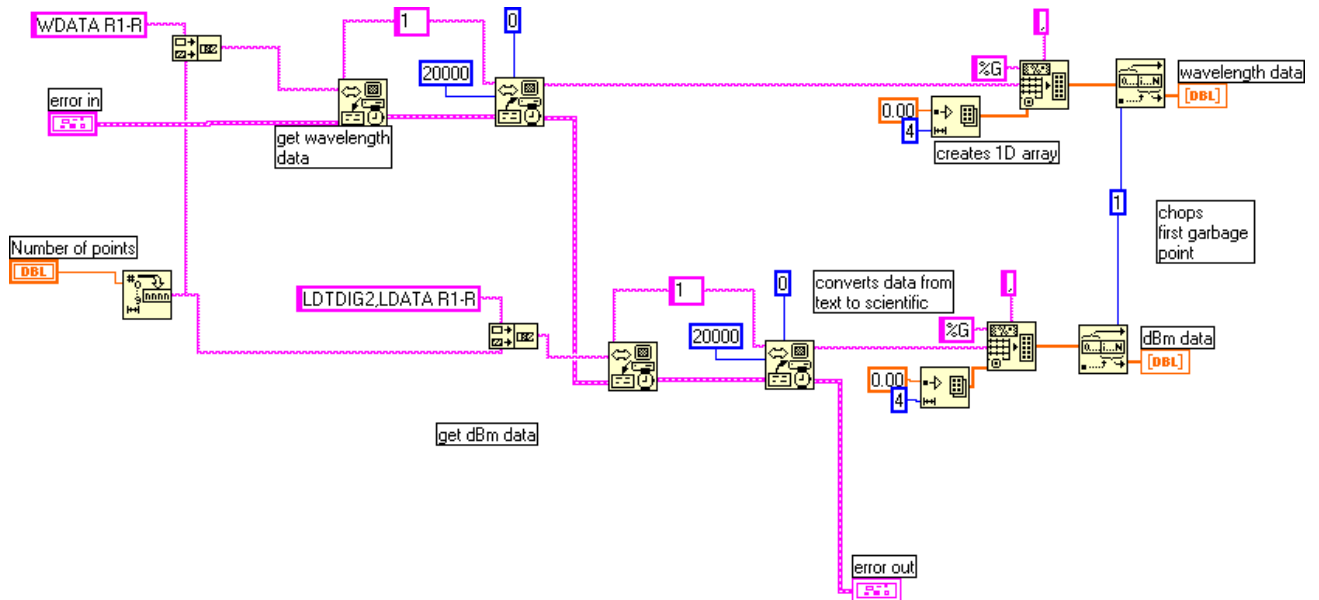


## A.4 SimSidelobe.vi

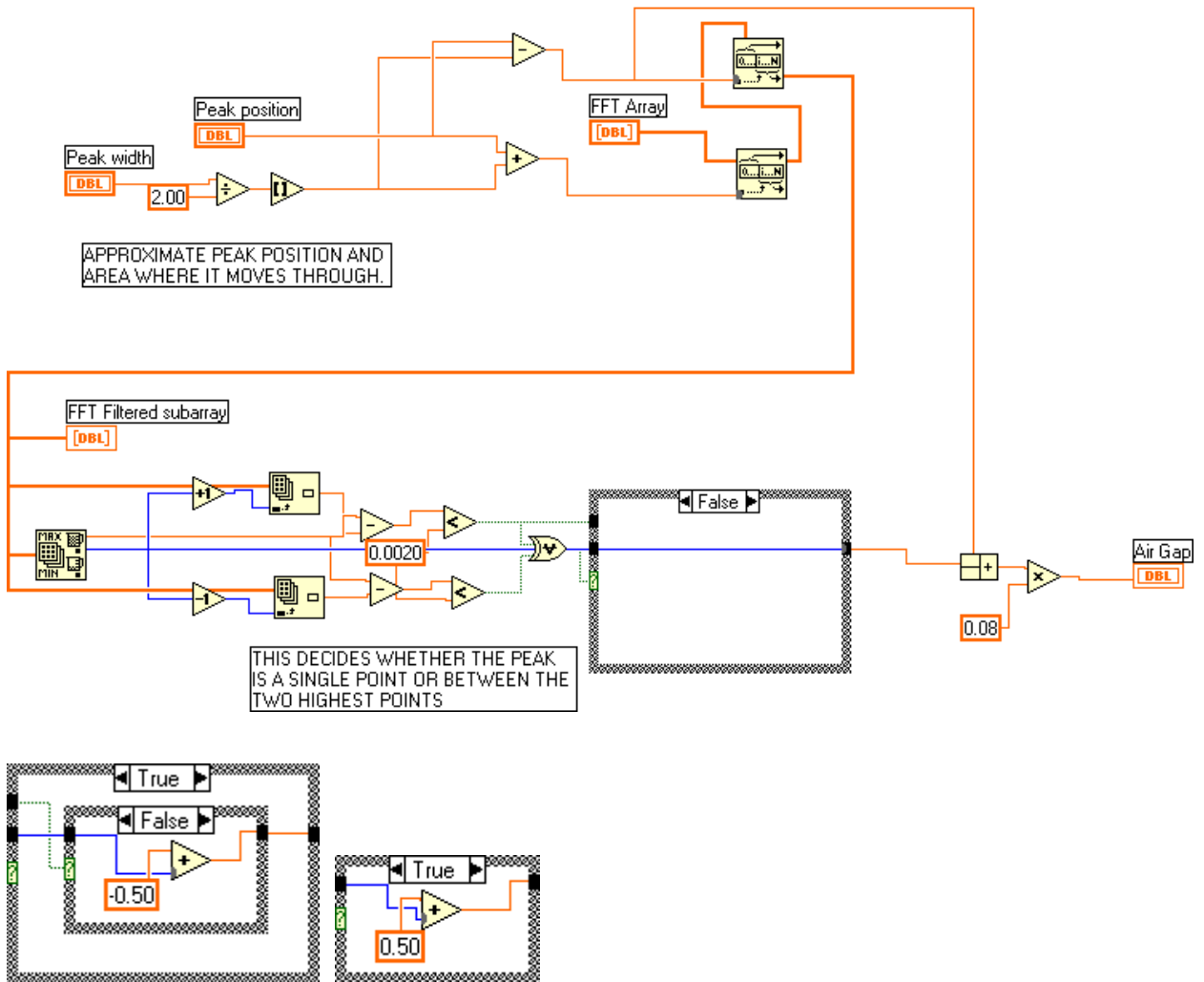## Connector Pane

# Block Diagram



# A.5 Filter.vi

A Simple filter program that has user input the approximate value of the peak and its width. The filter looks in the area for a peak and makes a decision on if it is at a single point or between two points.

# Connector Pane

## Block Diagram



Peak position

Peak width

2.00

APPROXIMATE PEAK POSITION AND
AREA WHERE IT MOVES THROUGH.

FFT Array

FFT Filtered subarray

0.0020

False

THIS DECIDES WHETHER THE PEAK
IS A SINGLE POINT OR BETWEEN THE
TWO HIGHEST POINTS

0.08

Air Gap

True

False

-0.50

True

0.50

# A.6 Simulation.vi

This VI generates a theoretical spectrum and takes the FFT of it. The peak of the FFT is found and plotted verse the gap used to create it. The loop is repeated for air-gaps over 200 microns. The data is saved as 1D arrays in text files to be plotted in Microsoft Excel.

## Block Diagram

300 N
1000 N
1000
2π
2.0
1230
i
0.16000
5
i
2
ℱ(x)
re im
DBL
MAX MIN
cos

c:\data\simpeaks.txt
12.3 TXT

XY Graph

C:\data\simgap.txt
12.3 TXT
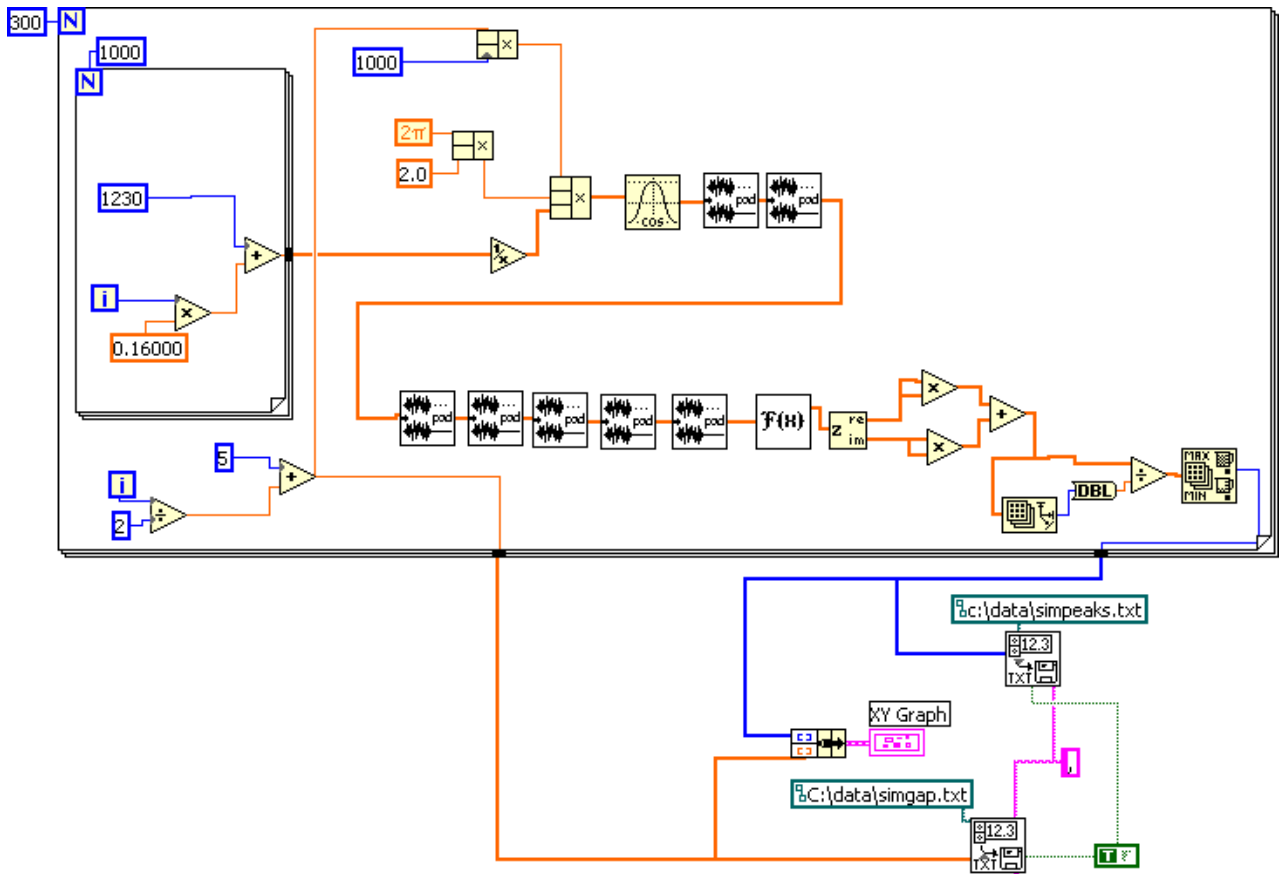
# References

1   George R Strakosch, *The Vertical Transportation Handbook.* John Wiley and Sons, NY, Third Edition, 1998.

2   Edward A. Donoghue, *Handbook on A17.1 Safety Code for Elevators and Escalators*, The American Society of Mechanical Engineers, 1982.

3   Micheal Gedeon, "Technical Tidbits", Brush Wellman Engineered Materials, Vol 3, no. 4, April 2001.

4   G.S. Holister, *Developments in Stress Analysis-1,* Applied Science Publishers LTD, London, 1979.

5   E.J. Hearn, *Strain Gauges*, Merrow Publishing Co. LTD, England, 1971.

6   James J. Brophy, *Basic Electronics for Scientists*, McGraw-Hill, NY, 1966.

7   Alex T. Edwards, "Comparison of Strain Gauge and Fiber Optic On A Sting Balance In A Supersonic Wind Tunnel", *Master's Thesis*, Virginia Polytechnic Institute and State University, Blacksburg, VA, 2000.

8   Ajoy Ghatak and K. Thyagarajan, *Introduction to Fiber Optics*, Cambridge University Press, 1998.

9   D.A. Krohn, *Fiber Optic Sensors: Fundamentals and Applications*, Instrument Society of America, NC, 2000.

10  Peter M. Tracey, "Intrinsic Fiber-Optic Sensors", *IEEE Transactions on Industry Applications*, Vol 27, no. 1, January, 1991.

11  John Dakin and Brian Culshaw, *Optical Fiber Sensors: Principles and Components*, Artech House, Norwood, MA, 1988.

12  M.H. Maher and E. G. Nawy, "Evaluation of Fiber Optic Bragg Grating Strain Sensor in High Strength Concrete Beams", *Application of Fiber Optic Sensors in Engineering Mechanics*, American Society of Civil Engineers, NY, 1993.

13  V. Bhatia, M.B. Sen, K.A. Murphy, and R.O. Claus, "Wavelength-tracked white light for highly sensitive strain and temperature measurements", *Electronic Letters*, Vol 32, no. 3, February, 1996.

14  A. Diez, G. Kakarantzas, T.A. Birks, and P.St.J. Russell, "High Strain Induced Wavelength Tunability in Tapered Fiber Acousto-Optic Filters", *Electronic Letters*, vol 36, no 14, July 6th 2000.

15  S.R. Taplin, and D.A. Jackson, "Multiplexing Schemes for Whitelight Channeled Spectrum Technique", *The Institution of Electrical Engineers*, Savoy Place, London, 1995.

16  Theodore S. Rappaport, *Wireless Communications: Principles and Practice*, Prentice Hall PTR, NJ, Second Edition, 2002.

17  Govind P. Agrawal, *Fiber-Optic Communication Systems*, John Wiley and Sons Inc, Second Edition 1997.

18  A.D. Kersey, A. Dandridge, and M.A. Davis, "Code-division Multiplexed Interferometric Array With Phase Noise Reduction And Low Crosstalk", *8th Optical Fiber Sensors Conference*, The Institute of Electrical and Electronics Engineers, Inc, 1991.

19  Athanasios Papoulis, *Probability, Random Variables, and Stochastic Processes*, McGraw-Hill, Third Edition 1991.

20  J.L. Santos, A.P. Leite, D.A. Jackson, "Optical fiber sensing with a low finesse Fabry-Perot cavity", Vol 31, no. 34, pg. 7361, December, 1992.

# Vita

David Christopher Geib was born in Huntington, New York on January 31$^{st}$, 1979. He graduated with a Bachelors of Science in Physics from State University of New York College at Geneseo in May 2001. He then continued on at Virginia Tech and received his Master's Degree in Electrical Engineering with a focus in communications in August 2003.